

Mathematical Research with Technology

Visualization of Gauss-Bonnet Theorem

Yoichi Maeda

maeda@keyaki.cc.u-tokai.ac.jp

Department of Mathematics

Tokai University

Japan

Abstract: The sum of external angles of a polygon is always constant, 2π . There are several elementary proofs of this fact. In the similar way, there is an invariant in polyhedron that is 4π . To see this, let us consider a regular tetrahedron as an example. Tetrahedron has four vertices. Three regular triangles gather at each vertex. Developing the tetrahedron around each vertex, there is an *open angle*, π . The sum of these *open angles* is 4π . As another example, let us consider a cube. There are eight vertices and an *open angle* is $\pi/2$ at each vertex. The sum of *open angles* is also 4π . This fact is regarded as a discrete case of the famous Gauss-Bonnet theorem. Using dynamic geometry software *Cabri 3D*, we can easily understand a simple proof of this theorem. The key word is *polar polygon* in spherical geometry.

1. Introduction

Elementary school students know the sum of external angles of polygons as well as the sum of interior angles. The sum of external angles of polygons is always 2π . In this sense, polygon has an invariant. How about an invariant of polyhedron? That is the value of 4π . This is a special case of the famous Gauss-Bonnet theorem, however, we can easily show elementary school students this invariant. To see this, let us define *open angle* at first.

Definition 1.1(Open Angle of Polyhedron) Let V be a vertex of a polyhedron. Developing the polyhedron around the vertex V , there is an angle which forms 2π when joined together with the angles of faces gathering at V (Figure 1.1). We call this complementary angle *open angle* at the vertex V .

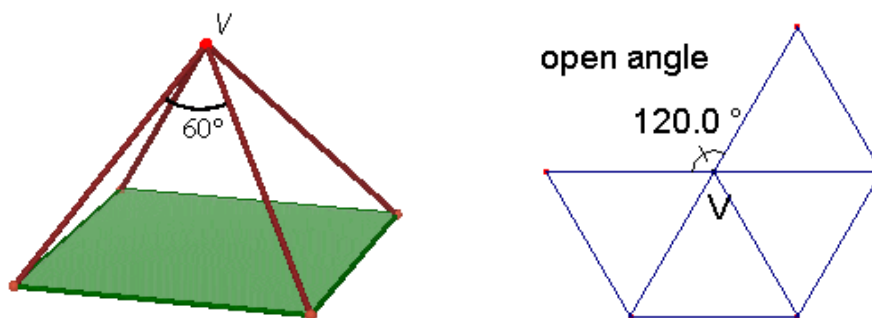


Figure 1.1 Pyramid and open angle at the top.

Using this open angle, we can easily show the invariant in polyhedron for elementary school students.

Figure 1.2 shows a regular tetrahedron and its net. Tetrahedron has four vertices, and three regular triangles gather at each vertex. The open angle at each vertex is equal to $\pi \left(= 2\pi - 3 \times \frac{\pi}{3} \right)$. The sum of open angles is 4π in this case.

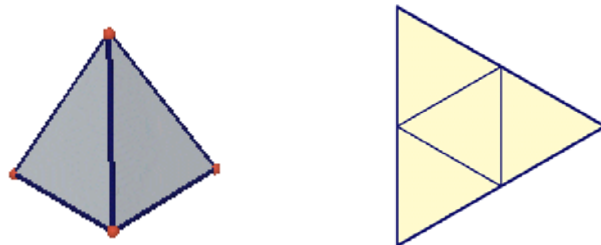


Figure 1.2 Tetrahedron and its polyhedral net.

The next example is a cube. Figure 1.3 shows a cube and its net. Cube has eight vertices, and three squares gather at each vertex. Flattening these three faces around each vertex on a plane, there exists an open angle $\frac{\pi}{2} \left(= 2\pi - 3 \times \frac{\pi}{2} \right)$ at each vertex. The sum of open angles is also 4π .

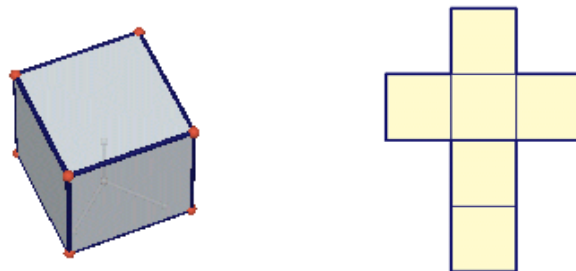


Figure 1.3 Cube and its polyhedral net.

The next one more example is sufficient for students to assent this invariant. Figure 1.4 shows an octahedron and its net. Octahedron has six vertices, and four regular triangles gather at each vertex. The open angle is $\frac{2\pi}{3} \left(= 2\pi - 4 \times \frac{\pi}{3} \right)$ at each vertex. The sum of open angles is 4π , too.

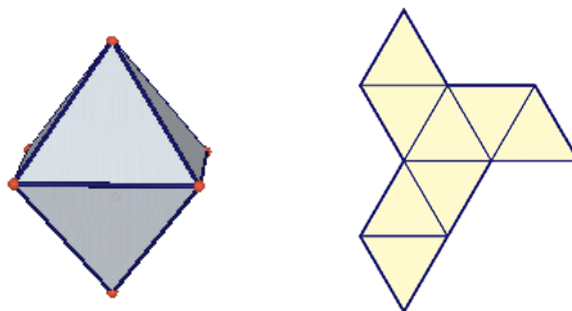


Figure 1.4 Octahedron and its polyhedral net.

At this stage, students want to know the reason why the sum of open angles is always constant. It is a little bit complicated to explain. In this paper, we will visualize this reason with dynamic geometry software *Cabri3D*. For simplicity, we assume that polyhedrons are convex and with no genres. We will recall the invariant in polygon in Section 2. Two intuitive proofs are provided, and both proofs are important for the explanation of the invariant of polyhedron. In Section 3, we will see intuitively that the invariant of polyhedron is 4π by fattening the polyhedrons.

Finally, we will see the relation between the open angles of polyhedron and the invariant. In this course, students will naturally gain a new understanding of difficult concepts: spherical geometry, duality, and curvature.

2. Invariant in polygon

In this section, we will review the invariant in polygon; the sum of external angles of polygon is always 2π .

One proof is showed in Figure 2.1(left). Imagine that a vector (or a pencil) moves along the convex polygon. At a vertex, the vector turns to the left with the external angle. When the vector returns to the start point, the vector has rotated just one time. Hence the sum of external angles is 2π . The external angle is regarded as the angle to flatten the vertex angle of the polygon on a straight line. In this sense, external angle in polygon may correspond to open angle in polyhedron.

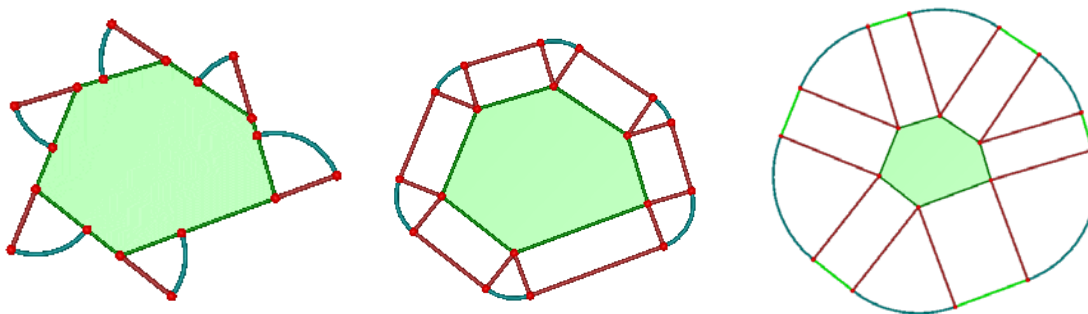


Figure 2.1 External angles(left) and Fattening polygons(center and right).

Another proof is to fatten the polygon in Figure 2.1(center). When we fatten a polygon, there is a circular sector at each vertex ([1] p.18). Here, let us prepare the following definition.

Definition 2.1(Outer Angle of Polygon) Let V be a vertex of a polygon. Fattening the polyhedron, there is a circular section at V . We call the central angle of the circular sector *outer angle* at the vertex V .

Outer angle does not depend on the size of the circular sector. Note that at each vertex, the outer angle is equal to the external angle. It is easy to see that outer angles form a whole disc, that is, our invariant. The more we fatten the polygon, the more the fattened polygon looks like circle as in Figure 2.1(right). In this way, we can see that circular sectors are deeply related to the invariant. This fact is useful when we consider the invariant in polyhedron in the next section.

3. Invariant as outer solid angles

In this section, let us consider to fatten polyhedrons, and discover the existence of an invariant in polyhedron.

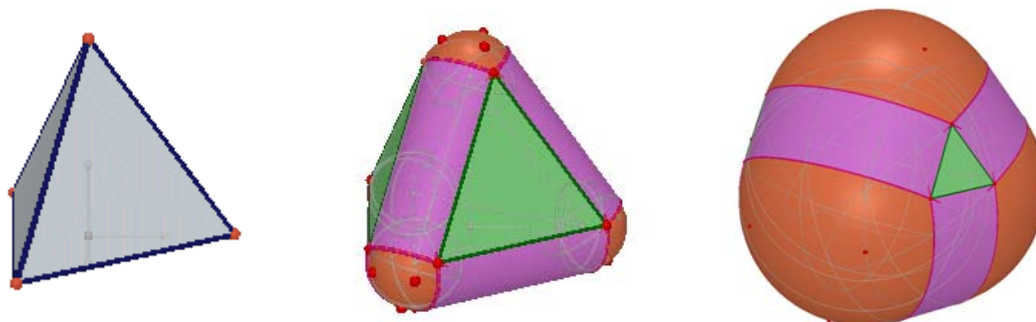


Figure 3.1 Fattening tetrahedron.

Figure 3.1 shows fattening of tetrahedron. We can see that there is a spheric sector at each vertex and their union form the ball ([1] p.19).

Definition 3.1(Outer Solid Angle of Polyhedron) Let V be a vertex of a polyhedron. Fattening the polyhedron, there is a spheric section at V . We call the solid angle of the spheric sector *outer solid angle* at the vertex V .

Outer solid angle does not depend on the size of the spheric sector. Outer solid angle is identified as the corresponding area of the unit sphere. Hence the sum of these outer solid angles is 4π . This value is our desired invariant. Figure 3.2 also shows fattening of cube. In the same way, eight spheric sectors at each vertex also form the ball.

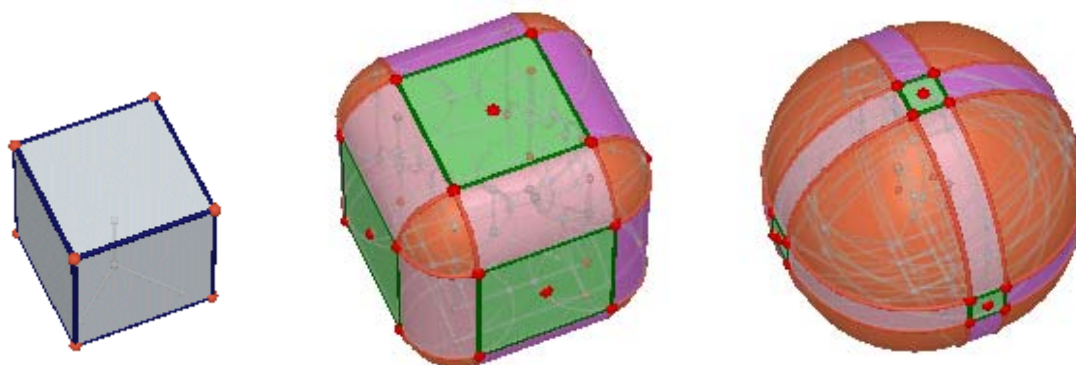


Figure 3.2 Fattening cube.

Our aim in the following argument is to show that this outer solid angle is equal to the open angle described in Section 1. In this context, we can say the relation among four angles symbolically;

$$\text{External angle} : \text{Open angle} = \text{Outer angle} : \text{Outer solid angle}.$$

4. Invariant as open angles

Once again, let us show two more examples. Figure 4.1 shows a dodecahedron and its net. Dodecahedron has twenty vertices, and three regular pentagons gather at each vertex. Flattening these three faces around each vertex on a plane, there exists an open angle $\frac{\pi}{5} \left(= 2\pi - 3 \times \frac{3\pi}{5} \right)$ at each vertex. The sum of open angles is 4π .

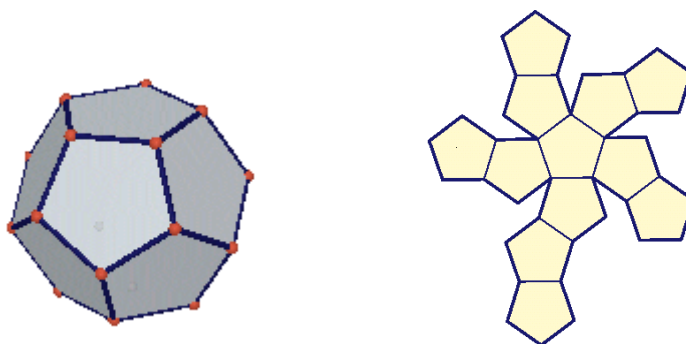


Figure 4.1 Dodecahedron and its polyhedral net.

Figure 4.2 shows an icosahedron and its net. Icosahedron has twelve vertices, and five regular triangles gather at each vertex. Flattening these five faces around each vertex on a plane, there exists an open angle $\frac{\pi}{3} \left(= 2\pi - 5 \times \frac{\pi}{3} \right)$ at each vertex. The sum of open angles is 4π , too.

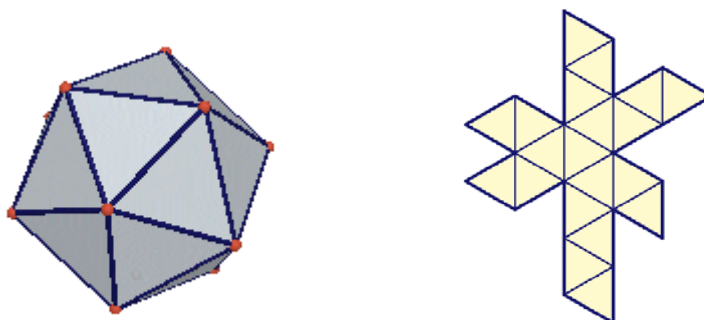


Figure 4.2 Icosahedron and its polyhedral net.

From Section 3, to proof the sum of open angles of a polyhedron is always equal to 4π , it is sufficient to show that the open angle is equal to the outer solid angle at each vertex. Since solid angle is defined as the spherical area in the unit sphere, in the following argument, we assume that spherical sectors are in the unit ball.

Figure 4.3 shows a vertex V with spheric sector $A'B'C'$. Spherical triangle $A'B'C'$ is called the polar triangle of spherical triangle ABC . These two triangles are mutually dual.

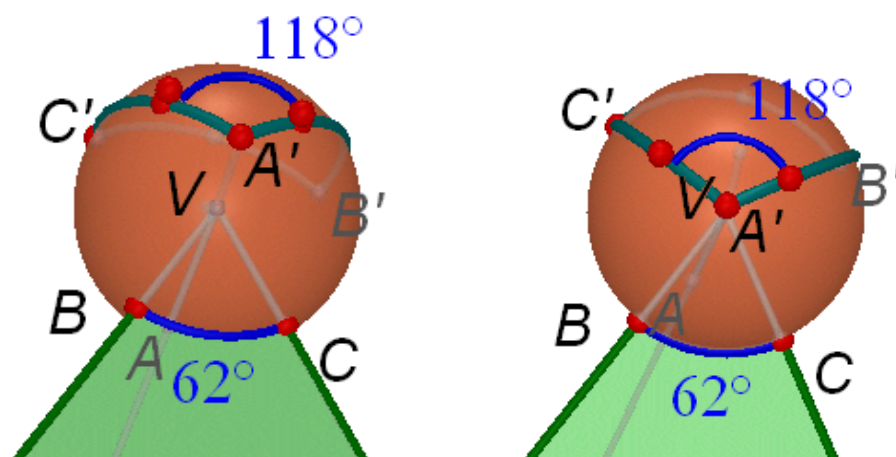


Figure 4.3 Spheric sector at a vertex.

In the picture above, point B is a pole of the great circle $C'A'$ (see, Figure 4.3(right)). In the same way, point C is a pole of the great circle $A'B'$, and so on. Then note that $\angle BVC = \pi - \angle A'$. It is similar to outer angle in Section 2. Here recall the Girard's formula; the area of a spherical triangle with angles α, β, γ is $\alpha + \beta + \gamma - \pi$ ([1] pp.278-279, [2] p.51).

Then, when three faces BVC , CVA , and AVB form the vertex V of a polyhedron,

$$\begin{aligned} \text{open angle at the vertex}(VABC) &= 2\pi - (\angle BVC + \angle CVA + \angle AVB) \\ &= 2\pi - ((\pi - \angle A') + (\pi - \angle B') + (\pi - \angle C')) \\ &= \angle A' + \angle B' + \angle C' - \pi \\ &= \text{area of spehrical triangle}(A'B'C') \\ &= \text{outer solid angle at the vertex}(VABC). \end{aligned}$$

More generally, we can show the following proposition.

Proposition 4.1(Open Angle and Outer Solid Angle) Let V be any vertex of convex polyhedron. The open angle at V is equal to the outer solid angle at V .

Proof. If n -faces A_1VA_2 , A_2VA_3 , ..., and A_nVA_1 form the vertex V ,

$$\begin{aligned} \text{open angle at a vertex}(VA_1A_2A_3 \cdots A_n) &= 2\pi - (\angle A_{n-1}VA_n + \angle A_nVA_1 + \angle A_1VA_2 + \cdots + \angle A_{n-2}VA_{n-1}) \\ &= 2\pi - ((\pi - \angle A'_1) + (\pi - \angle A'_2) + (\pi - \angle A'_3) + \cdots + (\pi - \angle A'_n)) \\ &= \angle A'_1 + \angle A'_2 + \angle A'_3 + \cdots + \angle A'_n - (n-2)\pi \\ &= \text{area of spehrical polygon}(A'_1A'_2A'_3 \cdots A'_n) \\ &= \text{outer solid angle at the vertex}(VA_1A_2A_3 \cdots A_n). \end{aligned}$$

■

In this way, we have proved that the sum of open angles of convex polyhedron is 4π .

5. Conclusions

In this paper, we introduce the invariant of open angles in polyhedron. It is not difficult for students to understand this invariant by using three-dimensional geometry software. In addition, it is founded out that the invariant in polyhedron is a natural extension of that in polygon. This invariant is applicable not only for regular polyhedrons and also general polyhedrons: concave polyhedrons or polyhedrons with genres. In this case, the value of invariant is equal to $2\pi\chi(M)$ where M is a polyhedron and $\chi(M)$ is the Euler Characteristic of M (Gauss-Bonnet theorem). Through this study, students will be interested in three-dimensional objects, spherical geometry, and more general Riemannian geometry.

References

- [1] Berger, M. (1977). *Geometry II*. Springer-Verlag Berlin Heidelberg.
- [2] Jennings, G. (1994). *Modern Geometry with Applications*. Springer-Verlag New York.

Generalizing 2D Geometric Properties to 3D With the Aid of DGS

Dohyun Kim

phy_kim@yahoo.com

Korea Science Academy

Korea

Hyobin Lee

rifyodeng@naver.com

Korea Science Academy

Korea

Seunguk Jang

910217j@hanmail.net

Korea Science Academy

Korea

Youngdae Kim

bigroadaz@hanmail.net

Korea Science Academy

Korea

Abstract: In this paper we would show how we could use computer programs in geometry researches. This paper contains the processes of generalizing the properties of 2D-geometry to that of 3D-geometry. Also, we would show how we could generalize backward; we could generalize further on 2D-geometry using the properties we found in 3D-geometry. In our research, we tried to generalize triangular properties into polygons and tetrahedrons. The computer tools we used are GSP and Cabri 3D. We used GSP for 2-dimensional researches and Cabri 3D for 3-dimensional researches.

1. Introduction

Geometry is able to be studied whenever we have things to draw, such as a sketch board. However, in this way of research using these boards, the accuracy is not assured. It means that it is hard to draw a figure exactly. It's even harder for 3-Dimensional figures. With a development of computer technology, drawing and visualizing these figures became much easier. It means that the accuracy and efficiency in geometry researches can be significantly improved.

In this paper, we used GSP to study 2D Geometry and Cabri-3D to study 3D Geometry. GSP is one of the most renowned computer tools around the world in studying 2D Geometry. However, Cabri-3D is not the one used frequently. Because it has been introduced lately, it is not yet familiar to people around the world.

This paper focused on giving examples of applying computer tools on geometry researches. In chapter 2, we showed how triangle centers are generalized to tetrahedrons. We described about generalizations of Menelaus' theorem to polygons and polyhedrons, and about backward

generalization, from polyhedrons to polygons in chapter 3. In chapter 4, we showed how we could find a property using dynamic methods of visualizing and performing experiments. We used a method of dynamic modeling using computer tools. We could precede our research very efficiently using computers. Our research was performed mainly by three steps.

First, using GSP, we studied about the two-dimensional properties in detail. Then, we inferred how it works on 2-dimensional planes. Also we fully understood through performing a number of experiments using computer tools.

Second, we tried to generalize 2D properties to 3D space. In this process, we used Cabri 3D. We could fully visualize and try a number of figures. It was very helpful for performing a research on them. Compared to the non-dynamic methods, it was much easier to study, analyze and visualize the figures. We hypothesized our results from the experiments.

Third, through proving those found properties, we could check our conjectures we made before and also we could explore the possibility of generalizing further. In addition, we could generalize backward.

With the aid of DGS and dynamic modeling method, the research proceedings become more efficient. Performing a lot of experiments, we could easily figure out how we can generalize the properties. With the ideas from experiments in 2D, we could apply those ideas easily on 3D. This really helped our flow of thoughts. Generalizing triangle centers, especially for orthocenters, we could perform a lot of trials and found proper conditions they exist. Also in chapter 3, since Menelaus' theorem is based on measurements of the line segments, we could calculate the results very effectively. If we hadn't those computer tools, we were not able to get results, because we have crucial difficulties on measuring distances on 3D. In addition, Fermat point in chapter 4 shows the method of trial/mistake approach. This is one of the best advantages of a research with computer tools.

2. Triangle Centers

1. Incenters, Excenters, Centroids and Circumcenters

The definition of the incenter of a triangle is a center of triangle's inscribing circle, and be constructed as a point where three angle bisectors intersect. For any points on the angle bisector is equidistant to the two sides. So, the point where three angle bisectors intersect is equidistant to the three sides. This means that it can be the center of the incircle.

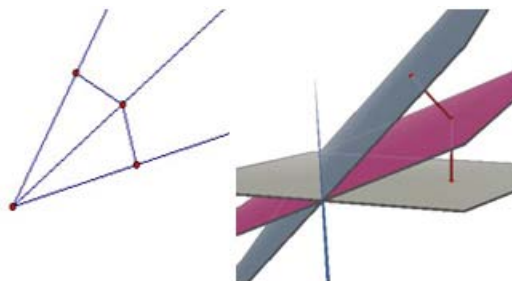


[Figure 2 - 1] An angle bisector and an interior-dihedral angle bisector plane

We directly extended this concept into 3D space. If we construct interior-dihedral angle (=inner angle made by planar sides of tetrahedron) bisector plane, this plane consists of points which has same distance from two planar sides (of tetrahedron). There, we can find 6 interior-dihedral angles

and drew six bisector planes for each angle. We deduced that the point would be equidistant to all facets of the tetrahedron if these six bisector planes intersect at a single point. Furthermore, this point would be the center of inscribing sphere, or insphere. We drew some figures and found that these six planes intersect at a single point and it is the center of the insphere.

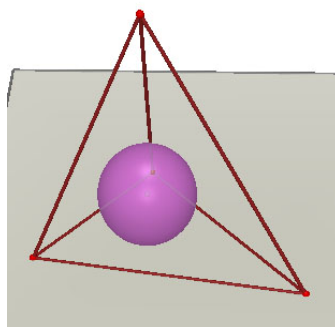


[Figure 2 - 2] The incenter of a tetrahedron

Next, we proved that these 6 bisectors meet on a single point. Then we also proved that it is center of insphere. Not only for incenter, but for circumcenter, centroid, and excenter, we had similar procedure. These 4 centers were easily generalized. For any tetrahedron, those 4 centers exist, and we succeeded to prove them. [Table 2-1] is indicating where those other 3 centers are and their properties.

[Table 2 - 1] Other centers of tetrahedron

Centers	Position in 2D Geometry	Position in 3D Geometry	Property
Circumcenter	A point where three perpendicular bisectors intersect	A point where perpendicular bisecting planes intersect	Becomes the center of the circumcircle and the circumsphere, respectively
Centroid	A point where three medians intersect	A point where median planes (Planes with a edge and its opposite edge's middle point) intersect	Divides the line which connects a point and the opposite planes' centroid as 2:1, 3:1 respectively
Excenter	A point where exterior angle bisectors intersect	A point where exterior dihedral-bisecting planes intersect	Becomes the center of the excircle and the exosphere, respectively

2. Orthocenters

The orthocenter of a triangle is a point where three altitudes intersect. Then, this time, we proceeded to the generalization directly.

We generalized directly to 3D, and we defined the orthocenter as the point where the four altitudes of a tetrahedron intersect. We drew several figures. However, we soon found that the four altitudes for general tetrahedrons don't intersect each other. Then we started from a regular tetrahedron. For a regular tetrahedron, the orthocenter existed. Using a dynamic modeling method, we checked if it can be generalized.

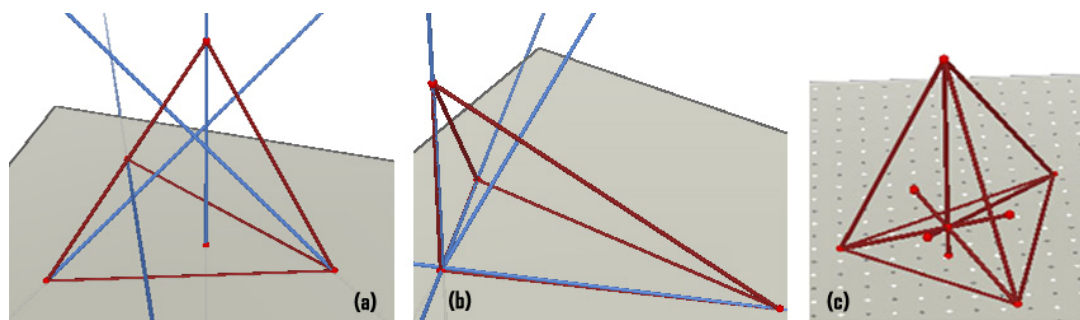


[Figure 2 - 3] (a) General tetrahedrons (b) A counter example of the conjecture (c) Orthocenter of a tetrahedron

First, we moved a point vertically up and down, and the center existed. Then, we made a conjecture that the orthocenter exists when at least one facet is an equilateral triangle. However we found some counter examples, as shown in [Figure 2-3(b)]. We precede our research to generalize this condition of equilateral triangle. Finally, through a number of experiments, we found the orthocenter of a tetrahedron exists when an altitude intersects with opposite plane’s orthocenter. With a set of experiments, we checked that the orthocenter exists under this condition.

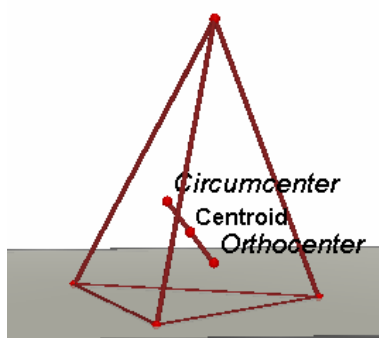


[Figure 2 - 4] Generalization of Euler's line

We proved that the four altitudes are concurrent on a point if at least one altitude intersects with the opposite plane’s orthocenter. Also, we proved that the four altitudes intersect with their opposite facet’s orthocenter if the orthocenter exists.

In addition, we’ve also shown that all orthotetrahedrons (=tetrahedrons with orthocenter) have circumcenter, centroid, and orthocenter to be collinear, as additional generalization of Euler’s line [Figure 2-4].

3. Menelaus’ Theorem

The following theorem was discovered by Egyptian mathematician Menelaus. This is what we will discuss in this whole chapter, and discuss about so-called “backward generalization” also.

Theorem(Menelaus) Given triangle ABC and a line l that never passes neither A nor B nor C, let D, E, F as intersection point between line l and line BC, CA, AB, respectively. Then,

$$\frac{BD}{DC} \frac{CE}{EA} \frac{AF}{FB} = 1$$

The proof is introduced in [Kay01], pp.320 and shall be omitted. To generalize it into polygon, we observed the equation $\frac{BD}{DC} \frac{CE}{EA} \frac{AF}{FB} = 1$, and found that:

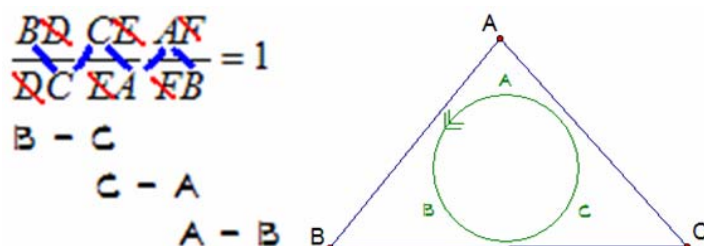


[Figure 3 - 1] Observing the pattern

That is, the vertices of triangle on the equation forms a “cycle”; namely, B-C-A. Keeping track of these points on triangle, we can see that it forms a cyclic curve. Also, between the points on cycle, we see that intersection point is placed on it (eg. Between B and C, there’s D; hence corresponding ratio is BD/DC).

1. Generalization to Polygons

By the observation done at the prior, we could conjecture that if we take circular track of polygon to multiply ratios of internal division by a fixed line, then we can get 1 as we did on triangle. To check it so, we’ve drawn [Figure 3-2]. To be specific, we state this theorem as following:

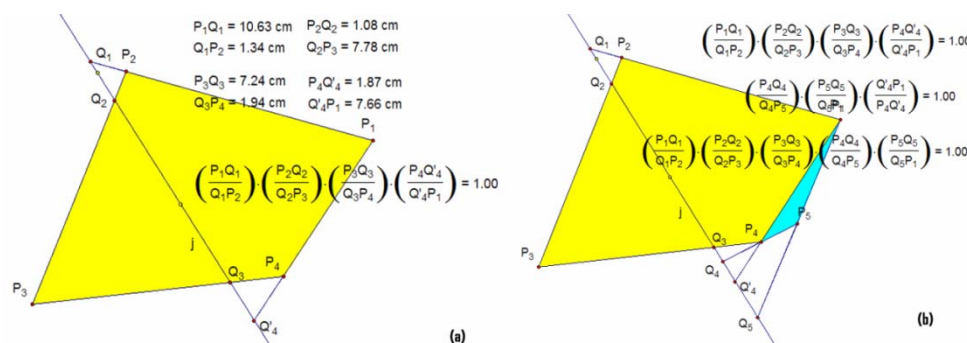


[Figure 3 - 2] Observation for generalization

At left side of [Figure 3-2], we noted that a an equation holds for quadrilaterals, namely¹

$$\frac{P_1Q_1}{Q_1P_2} \frac{P_2Q_2}{Q_2P_3} \frac{P_3Q_3}{Q_3P_4} \frac{P_4Q_4}{Q_4P_1} = 1$$

To extend it so, we added auxiliary triangle, one side “stuck” on former quadrilateral – see the right side of [Figure 3-2]. In this diagram, we observed that:

¹ In [Figure 3-2], P₁, P₂, P₃, P₄ all denotes vertices of yellow(big) quadrilateral. There’s line j passing through quadrilateral P₁P₂P₃P₄, and Q₁, Q₂, Q₃, Q₄ is intersection of line j with P₁P₂, P₂P₃, P₃P₄, P₄P₁ respectively. P₅ is auxiliary point added and Q₅, Q₄ denotes intersection of line j with P₅P₁, P₄P₅, respectively.

$$\frac{Q_4'P_1}{P_4Q_4'} \frac{Q_4P_4}{P_5Q_4} \frac{Q_5P_5}{P_1Q_5} = 1 \Rightarrow \frac{P_1Q_1}{Q_1P_2} \frac{P_2Q_2}{Q_2P_3} \frac{P_3Q_3}{Q_3P_4} \frac{P_4Q_4}{Q_4P_5} \frac{P_5Q_5}{Q_5P_1} = 1$$

It is a similar equation that is held in (general) pentagon. Employing this “recursive” or “inductive” idea, we found a general rule that holds for a n-gon. That is, given n-gon $P_1P_2\dots P_n$, and fixed line l (that never passes P_i), letting Q_i be intersecting point between line l and line P_iP_{i+1} , for $i=1, 2, \dots, n$ (define P_{n+1} as P_1), then we have:

$$\frac{P_1Q_1}{Q_1P_2} \frac{P_2Q_2}{Q_2P_3} \dots \frac{P_{n-1}Q_{n-1}}{Q_{n-1}P_n} \frac{P_nQ_n}{Q_nP_1} = 1$$

This equation is employed as our generalization of Menelaus’ Theorem at polygons.

2. Generalization to 3D

The idea of "cycle" takes central role in discovery of tetrahedral Menelaus' theorem. Though, Euler's contribution on graph theory tells us that we can't just loop through all edges for only once. Thus we can conclude that a full circular track can't be constructed on tetrahedrons. Though, when we just kept the idea of "closed loop" ONLY for tetrahedral generalization, we could obtain a result.

Suppose, for a tetrahedron ABCD, let $P_1P_2\dots P_nP_{n+1}$ be closed loop on that tetrahedron (so that $P_{n+1}=P_1$, P_i 's are either A, B, C, or D, and $P_i \neq P_{i+1}$). Given plane π that never passes A, B, C, nor D, let $Q_{i,i+1}$ be intersecting point between π and line P_iP_{i+1} .

Further, let h_i is height from P_i to π . Accompanying [Figure 3-3] (b), we can see that triangle $P_iH_iQ_{i,i+1}$ and $P_{i+1}H_{i+1}Q_{i,i+1}$ is similar and $P_iH_i = h_i$, $P_{i+1}H_{i+1} = h_{i+1}$ and, $P_iQ_{i,i+1} / Q_{i,i+1}P_{i+1} = h_i / h_{i+1}$ in conclusion. If we multiply this equation through $i=1$ to n , we obtain:

$$\frac{P_1Q_{1,2}}{Q_{1,2}P_2} \frac{P_2Q_{2,3}}{Q_{2,3}P_3} \dots \frac{P_{n-1}Q_{n-1,n}}{Q_{n-1,n}P_n} \frac{P_nQ_{n,1}}{Q_{n,1}P_1} = 1$$

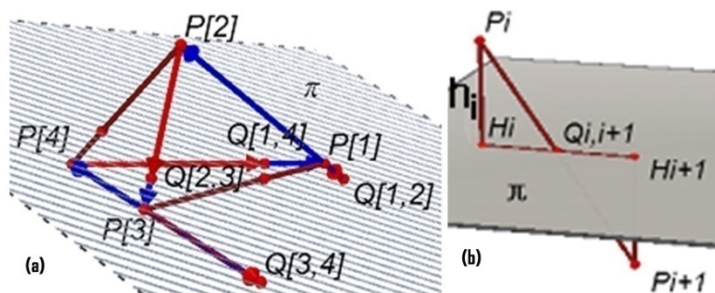
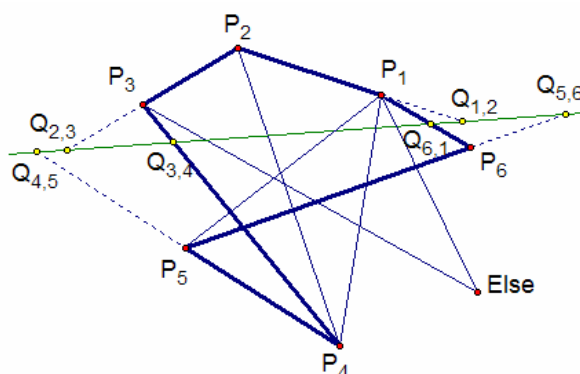


[Figure 3 - 3] (a) Menelaus' theorem for tetrahedrons (b) Height diagram

This equation is what we will now say Menelaus’ theorem for tetrahedrons. Although nowadays one can check this numerically with Cabri 3D but when we tried to observe this fact, Cabri 3D didn’t provided numerical calculation and therefore all we could do was finding an approach to proof.

3. Backward Generalization



$$\left(\frac{P_1Q_{1,2}}{Q_{1,2}P_2}\right)\left(\frac{P_2Q_{2,3}}{Q_{2,3}P_3}\right)\left(\frac{P_3Q_{3,4}}{Q_{3,4}P_4}\right)\left(\frac{P_4Q_{4,5}}{Q_{4,5}P_5}\right)\left(\frac{P_5Q_{5,6}}{Q_{5,6}P_6}\right)\left(\frac{P_6Q_{6,1}}{Q_{6,1}P_1}\right) = 1.00$$

[Figure 3 - 4] Result of Backward-generalization

Note that Theorem 3.3 has alike equation but the points stated are not as the same situation as the points stated in Theorem 3.2. In Theorem 3.2, the point P_i 's are aligned all vertices of polygon, but in Theorem 3.3, the point P_i 's are aligned not all vertices on tetrahedron and therefore can be redundant. Though, cancellation of height is achieved by similarity of right triangles and therefore can be achieved in planar geometry and planar loop of vertices as well. This achieved our backward-generalization, and stated as following [Figure 3-4]:

Think of a graph (diagram with points and segments, on Euclidean metric) K on a plane and a line ℓ (on the same plane) such that it never passes points of K . Think of cycle (=path that has same starting point and endpoint) $P_1P_2\dots P_nP_{n+1}$ on K , and suppose line P_iP_{i+1} meets with ℓ at $Q_{i,i+1}$. Then,

$$\frac{P_1Q_{1,2}}{Q_{1,2}P_2} \frac{P_2Q_{2,3}}{Q_{2,3}P_3} \dots \frac{P_{n-1}Q_{n-1,n}}{Q_{n-1,n}P_n} \frac{P_nQ_{n,1}}{Q_{n,1}P_1} = 1$$

4. Fermat Point

This chapter will discuss about advanced picturesque (or “colorful”) method of quantities using GSP and further usage of this. Before we go on, we will first give formal definition of “quantity” that we will use so far.

Suppose we have subset D of \mathbb{R}^2 . We may consider a map $f : D \rightarrow \mathbb{R}$ that we will call **quantity map** and the real number $f(P)$ will be called **quantity** at point P . Now to say how this concept is established in GSP, we just pick any point P from D , and if necessary, take some measurements among these points (static points may be included during this procedure), and calculate these measurements to gain a quantity at P (with a quantity map also). In addition, a **continuous quantity** is defined as a quantity from a continuous quantity map.

What we can do with GSP about the quantity is that they produce varying colors of figures – color of point, line or its segment, polygon area, etc. – as the function of (given) quantity, or **controlling quantity**. Furthermore, if we trace a figure with varying color, it leaves its *former* color in their former positions (and therefore traces are static unless it's drawn once again). To implement it so, the detailed procedure is stated below [Figure 4-1].

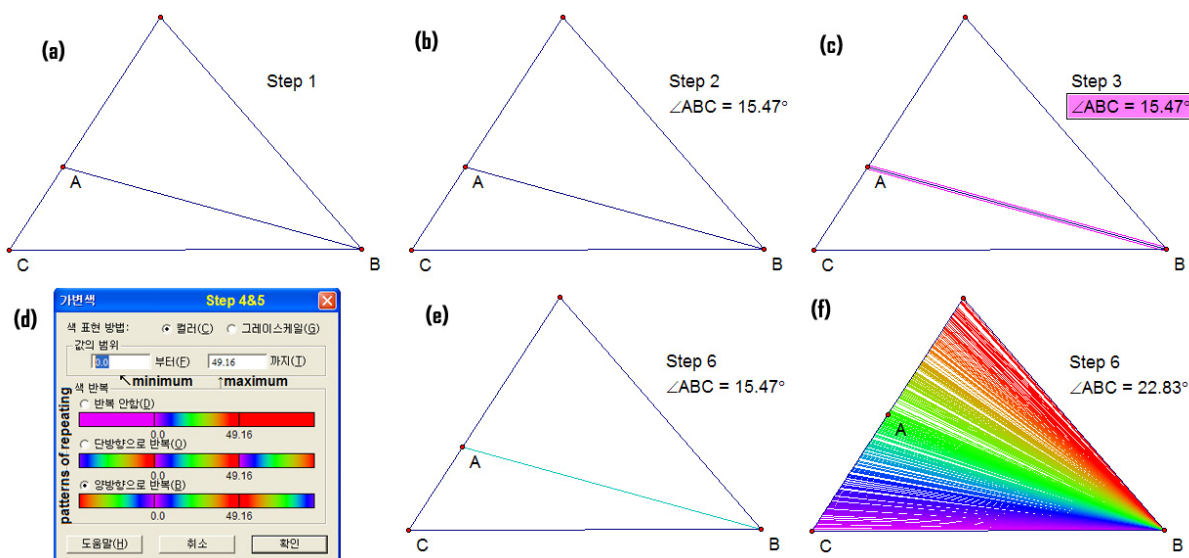


[Figure 4 - 1] Specific procedure of color conventional method

Step 1 – Draw a figure whatever you want to investigate. [(a)]

Step 2 – Give a quantity that you want to set as the controlling quantity. [(b)]

Step 3 – Select color-varying object and controlling quantity. [(c)]

Step 4 – Keeping the selection, go to View → Color → Varying color menu. [(d)]

Step 5 – Set the maximum, minimum value for repeating interval; be sure to notice what can be the maximum value and minimum value of controlling quantity in your figure. Set patterns of repeating if required. [(d)]

Step 6 – Now see how your varying-color object changes its aspect. If you need tracing it, you can turn on its tracing mode and see varying-color trace also. [(e),(f)]

Although example in [Figure 4-1] is giving traces of line segment, some specific cases that we usually deal with will trace a point P in domain D, with varying color which has its controlling quantity map from D and quantity at P. This kind of traces throughout D will be called **quantity variation trace**. See [Figure 4-2] for example, which has 2 traces for the same quantity map $f : D = \text{Inferior of } \triangle BCD \rightarrow \mathbb{R}, P \rightarrow BP + CP + DP$, and all of our varying-color traces will be assumed as a quantity variation traces from now on.

The most crucial part of this method is Step 5, setting repeating interval. The appropriate settings of this will enhance analysis of quantity variation trace of provided quantity map. If one sets repeating interval very similar to the same as range of quantity map, then one will see a **single color band**, or a single spectrum, from the point of minimum to the point of maximum. This kind of band is useful to see where the minimum or maximum value of quantity roughly exists, and to what direction is quantity rising; closely related with the concept of gradient as well. See the left side of [Figure 4-2] – one would find out that $BP+CP+DP$ will have its minimum value somewhere in the middle of the triangle, and it increases as P moves to the boundary of triangle.

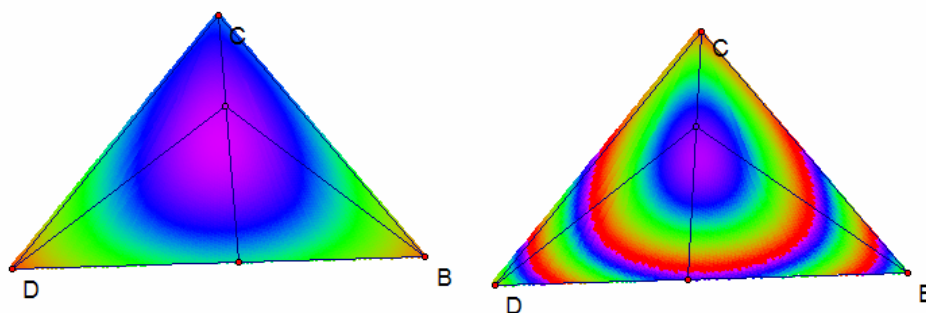


[Figure 4 - 2] Comparison between single color band & multiple color bands

For approximating quantities or figuring out more precisely where critical point exists, we should set repeating interval fairly small. If so, we find that variance of quantity may be shown as **multiple color bands**, that is, we may see multiple spectra of colors throughout the domain [Figure 4-2, right side]. The advantage of this is that we can resolute spectra more clearly. If continuity is assumed, then one can estimate which color band will represent which value of quantity, and moreover, one can figure out at which point will quantity map has its extreme values more clearly relative to single color band.

In the rest of this chapter, we will give an example of using quantity variation trace in geometric foundations. In specific, we will apply it to search of Fermat's point, or, finding a point F that minimizes $AF+BF+CF$, for given $\triangle ABC$. There, all we have to do is examining a quantity variation trace, with quantity at P as $AP+BP+CP$ and domain as $\triangle ABC$.

But there's one thing that we should be aware of; this picturesque method is a bit hard to find critical point directly from traces. This trace is no more than relying on person's sight, so our best information about critical point from traces is that *the point exists possibly around somewhere*(=**critical site**), and this information is valid for continuous quantity only.

Therefore, using traces to find critical points should be no more than auxiliary tool of theoretical construction of critical points of continuous quantities. Fortunately, for planary point P, we have $AP+BP+CP$ as continuous quantity, and for A, B, C satisfying certain conditions, we can geometrically construct critical point P inside $\triangle ABC$. So, we used traces to check validity of this geometrically constructed Fermat's point as an application, and in final, we succeeded.

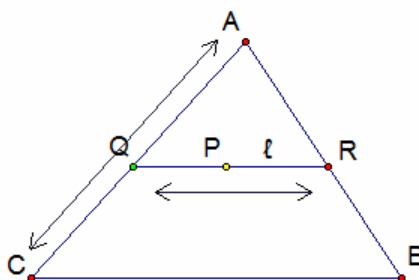


[Figure 4 - 3] Method for sweeping all points in triangle

There're two problems that we have to solve to do such works:

1. How we can check all points in $\triangle ABC$ for tracing?
2. How we can solve problem 1 efficiently?

Though, because we're mainly concerned with problems of possibility only, so we will not be concerned for problem 2.

The answer for problem 1 is quite easy. We pick a point on AC, say Q, and draw a line ℓ parallel to BC and passes Q. This will yield point R of intersection between ℓ and AB. Now we set another point, say P, roaming around the segment QR. We can easily find that P can cover every points of triangle if both Q and P moves truly arbitrarily on their domains [Figure 4-3].

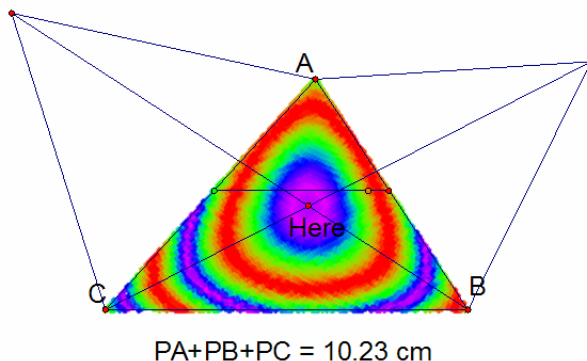


[Figure 4 - 4] Fermat's point & color band of quantity $AP+BP+CP$

The trace result of [Figure 4-3] is shown as [Figure 4-4], with repeating interval (9.85, 10.35).

We indicated in [Figure 4-4] as “Here” for geometrically constructed Fermat’s point. Note the area around point “Here” we can see that color bands are becoming bigger in their sizes, which is the important aspect of critical site. Therefore, we can see that [Figure 4-4] successfully gives validity of constructed Fermat’s point. Moreover, although we won’t discuss about the details, this method can be generalized for checking answers of general geometric optimization problems.

5. Conclusion

In summary, this paper contains generalizations of some triangle centers to tetrahedrons, and Menelaus' theorem, which introduced backward generalizations from 3D to 2D, and shows the process of finding Fermat point of a triangle.

Hence what we ultimately proposed in this paper is giving a specific example that shows how computer technique can help an extension of thought. For the example, we chose generalization of 2D-geometric property into 3D-geometric property. First, we chose geometry because it consists of studying our everyday figure, and, second, we chose generalization because it's simplest extensive thought upon the knowledge. The approach we used was dynamic modeling method using DGS. This way of study was very efficient and effective in research. We provided three example sub-studies using this method. In chapter 2, we provided an example of extending ideas directly from 2D to 3D. In addition, chapter 3 includes the capability of measuring in 3D, which can be impossible if we didn’t use Cabri 3D. Also in chapter 4, we showed trial/mistake method of research and optimizing the tools in studying.

For decades, computer became one of the most important tools in human’s daily lives. This means computers are interacting with people. As shown in this research, we showed computers effectively interact with researchers in mathematics. Through this study, we look forward to the future computer tools, both CAS and DGS, significantly interact with researchers and help their studies.

Acknowledgements

The work of this paper was originally one of themes of Korea Science Academy's Research & Education program in 2006. The authors, who were the participant students of the theme, express their special thanks to Choi, Jonsul from Korea Science Academy, Kim, Buyun from Busan University and Jung, Jaehun in Kimhae Sammun High school for helping their works in 2006.

References

[Kay01] David C. Kay, *College Geometry : A Discovery Approach 2nd Ed.*, Addison Wesley Longman, 2001.

The arbelos, mathematics and computer graphics

Hiroshi Okumura and Masayuki Watanabe

okumura@maebashi – it.ac.jp
Department of Life Science and Information
Maebashi Institute of Technology
Japan

watanabe@maebashi – it.ac.jp
Department of Integrated Design Engineering
Maebashi Institute of Technology
Japan

Abstract. The arbelos is a plane figure formed by three mutually touching circles with collinear centers. The figure is a historical one, but there are still many discoveries and ongoing researches for this today, which give comprehensible examples of development of mathematics and also give good geometric computer animation materials.

1. Introduction

Each of the areas surrounded by three mutually touching circles with collinear centers is called an arbelos or a shoemaker's knife (Figure 1). The arbelos has many charming properties and seems to be one of the most famous plane figures. It has often been used in problem solving journals and mathematics competitions.

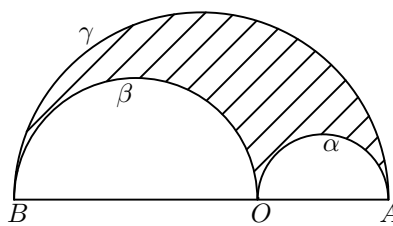


Figure 1

The arbelos was studied by Archimedes and Pappus, and has been considered as a historical figure. On the other hand, there are still many discoveries and ongoing researches for this figure today. In this article we show

that those recent researches give comprehensible examples of development of mathematics and also give good geometric computer animation materials.

2. Recent results on the arbelos

2.1. Archimedean circles

Let O be a point on the segment AB and let us consider one of the arbeloi formed by three circles α , β and γ with diameters AO , BO and AB , respectively. Among the many properties of the arbelos, the twin circle property seems to be one of the most famous one: Let us draw the tangent of the circles α and β at the point O . The arbelos is divided into two curvilinear triangles by this tangent, and the two incircles are congruent (Figure 2). Archimedes considered those two circles in his *Book of Lemmas*, and the circles are called the twin circles of Archimedes.

A circle congruent to the twin circles is said to be Archimedean. Leon Bankoff found that the circle passing through the tangency points of α , β and the incircle of the arbelos are Archimedean (Figure 3) [1]. He also pointed out the existence of one more Archimedean circle, the maximal inscribed circle in the lune made by γ and the common tangent of α and β , later (Figure 4) [2].

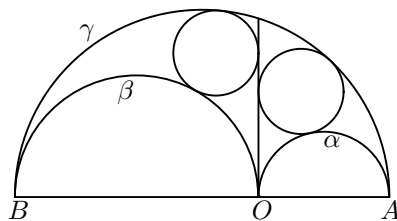


Figure 2

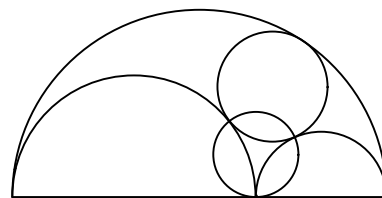


Figure 3

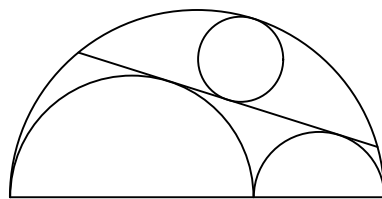


Figure 4

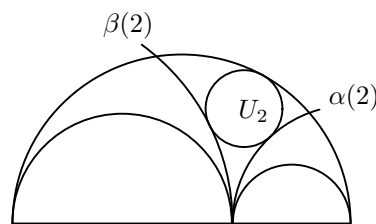


Figure 5

Let $(2a, 0)$ and $(-2b, 0)$ be the coordinates of the points A and B on the x -axis with the origin O for positive real numbers a and b . Recently dozen of

Archimedean circles were found [3]. Let $\alpha(z)$ and $\beta(z)$ be circles with centers $(za, 0)$ and $(-zb, 0)$ passing through O for a real number z . Thomas Schoch has found that the circle touching $\alpha(2)$ and $\beta(2)$ externally and γ internally is Archimedean (Figure 5). Peter Woo called the Schoch line the one passing through the center of this circle and perpendicular to the x -axis, and found that the circle U_z touching the circles $\alpha(z)$ and $\beta(z)$ externally with center on the Schoch line is Archimedean for a nonnegative real number z (Figure 6).

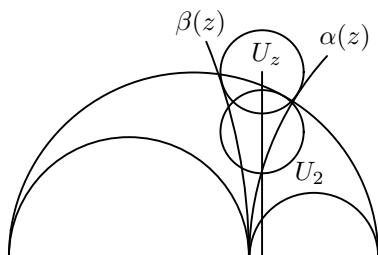


Figure 6

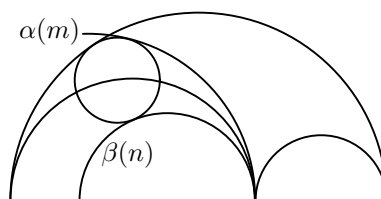


Figure 7

We say a circle touches $\alpha(z)$ appropriately if they touch externally (respectively internally) for a positive (respectively negative) number z . If one of the two circles is a point circle and lies on the other, we also say that the circle touches $\alpha(z)$ appropriately. The same notion of appropriate tangency applies to $\beta(z)$. The center of similitude of $\alpha(z)$ and γ is the external center of similitude of the two if $z > 0$ and the internal center of similitude if $z < 0$. The center of similitude of $\beta(z)$ and γ is defined similarly. Okumura and Watanabe have generalized Schoch's Archimedean circle as follows (see Figure 7) [4].

Theorem 1. *The following statements are equivalent for nonzero real numbers m and n .*

(i) *A circle touches $\alpha(m)$ and $\beta(n)$ appropriately and γ internally is Archimedean.*

(ii)

$$\frac{1}{m} + \frac{1}{n} = 1. \tag{1}$$

(iii) *The center of similitude of $\alpha(m)$ and γ coincides with the center of similitude of $\beta(n)$ and γ .*

Each of the twin circles of Archimedes can be obtained when $(m, n) \rightarrow (\pm\infty, 1)$ or $(m, n) \rightarrow (1, \pm\infty)$, and Schoch's Archimedean circle can be obtained when $(m, n) = (2, 2)$.

The radii of Archimedean circles is

$$r_A = \frac{ab}{a + b}.$$

And the Schoch line is given by

$$x = \frac{b - a}{b + a} r_A.$$

Okumura and Watanabe have shown the following [9]:

Theorem 2. *Let s and t be real numbers such that $tb \pm sa \neq 0$. If there is a circle of radius r touching the circles $\alpha(sz)$ and $\beta(tz)$ appropriately for a real number z , then its center lies on the line*

$$x = \frac{tb - sa}{tb + sa} r.$$

Schoch line is obtained when $t = s = 1$ and $r = r_A$. Woo's Archimedean circles seems to be an infinite set of Archimedean circles appeared for the first time in the history of Archimedean circles, but Theorem 2 shows that the property of those Archimedean circles does not hold only for Archimedean circles but circles with any radii.

The incircle of the curvilinear triangle determined by α and the tangents of β from the point A is Archimedean (Figure 8) [3]. This can be generalized as follows (Figure 9) [8].

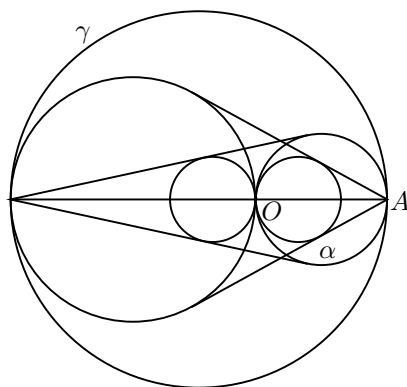


Figure 8

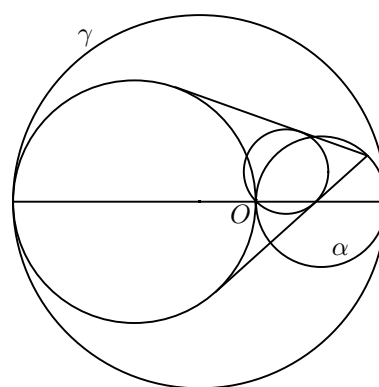


Figure 9

Theorem 3. A circle passing through O (not tangent internally to β) is Archimedean if and only if its external common tangents with β intersect at a point on α .

Let O_γ be the center of the circle γ . Frank Power has shown that for “highest” points P and Q on α and β respectively, the circles touching γ and the line $O_\gamma P$ (respectively $O_\gamma Q$) at P (respectively Q) are Archimedean (Figure 10) [11]. Let I be one of the intersections of γ and the perpendicular of AB passing through O , and let δ be a circle contained in γ and touching γ at I . Let the tangents of δ perpendicular to AB intersect α and β at P and Q respectively. The radius of δ is expressed by $k(a + b)$ for a real number k satisfying $0 \leq k < 1$. Power’s Archimedean circles can be generalized as follows (Figure 11) [7]:

Theorem 4. The radii of the circles touching the circle γ and the line $O_\gamma P$ (respectively $O_\gamma Q$) at the point P (respectively Q) are $2(1 - k)r_A$.

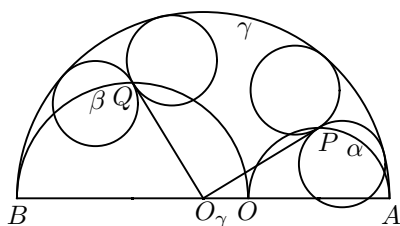


Figure 10

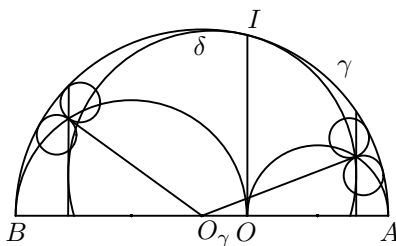


Figure 11

Power’s Archimedean circles can be obtained when $k = \frac{1}{2}$.

2.2. The arbelos in n -aliquot parts

Let $\alpha_0 = \alpha, \alpha_1, \dots, \alpha_n = \beta$ be $n + 1$ distinct circles touching α and β at O , where $\alpha_1, \dots, \alpha_{n-1}$ intersect γ and one of them may be the line perpendicular to AB passing through O . If the n inscribed circles in the curvilinear triangles bounded by $\alpha_{i-1}, \alpha_i, \gamma$ are congruent, we call this configuration of circles $\{\alpha, \alpha_1, \dots, \alpha_n = \beta, \gamma\}$ an arbelos in n -aliquot parts (Figure 12) [6]. The word “ n -aliquot” comes from the following property (Figure 13).

Theorem 5. Let $\{\alpha, \alpha_1, \dots, \alpha_n = \beta, \gamma\}$ be an arbelos in n -aliquot parts. If $n = pq$ for natural numbers p and q , then $\{\alpha, \alpha_q, \alpha_{2q}, \dots, \alpha_{pq} = \beta, \gamma\}$ is an arbelos in p -aliquot parts.

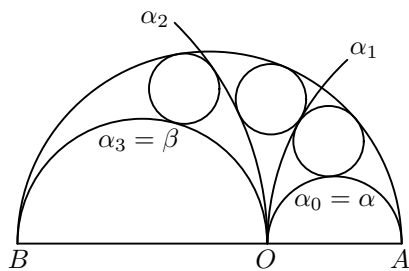


Figure 12 $n=3$

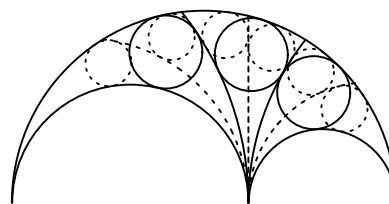


Figure 13 $p = 3, q = 2$

If $a \neq b$, the common radii of the inscribed circles in the n -aliquot arbelos is

$$\frac{ab(a^{\frac{2}{n}} - b^{\frac{2}{n}})}{a^{1+\frac{2}{n}} - b^{1+\frac{2}{n}}}$$

In an arbelos in n -aliquot parts, we can construct an arbelos in $(n+2)$ -aliquot parts (Figure 14).

Theorem 6. Let $\{\alpha, \alpha_1, \dots, \alpha_n = \beta, \gamma\}$ be an arbelos in n -aliquot parts. Let the circle γ' concentric to γ and touching the n congruent inscribed circles externally intersects AB at points A' and B' , where A' lies between A and O . If α_{-1} and α_{n+1} are circles with diameters OA' and OB' respectively, then $\{\alpha_{-1}, \alpha, \alpha_1, \dots, \alpha_n = \beta, \alpha_{n+1}, \gamma'\}$ is an arbelos in $(n+2)$ -aliquot parts.

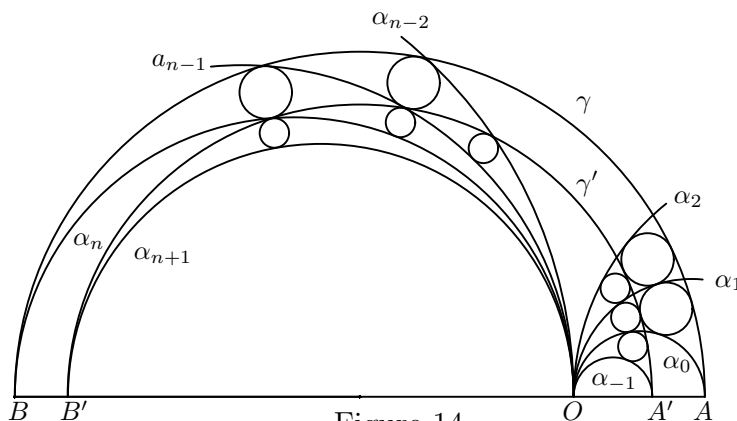


Figure 14

In an arbelos with its inscribed circle, we can construct an arbelos in 3-aliquot parts, and in it an arbelos in 5-aliquot parts, \dots . In this way we can get an embedded pattern of the arbelos, which may be called an odd pattern. In a similar way we can get an even pattern. Figure 15 shows several relationships between the two patterns.

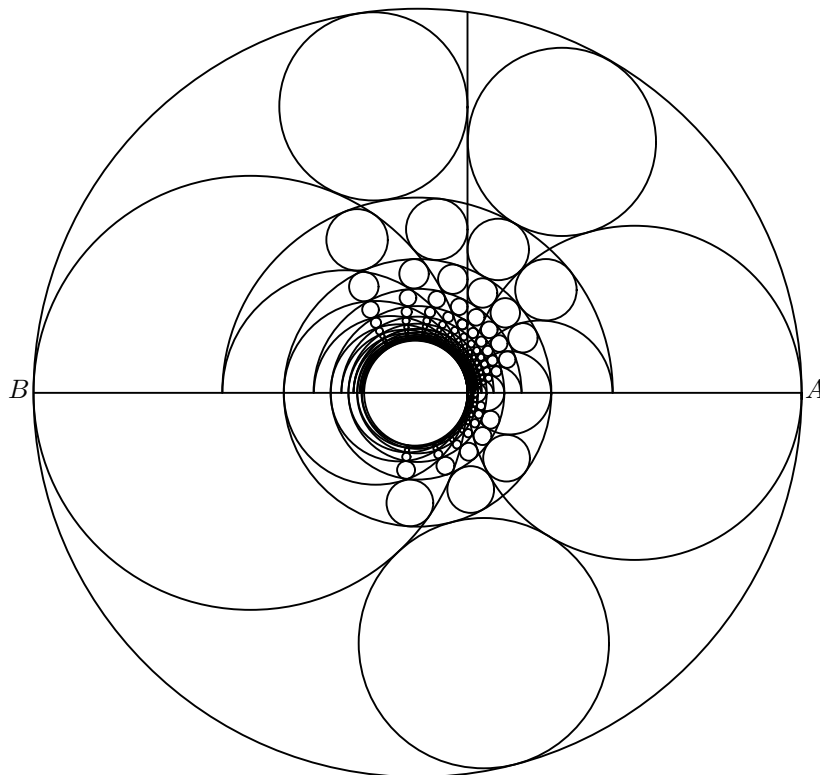


Figure 15

2.3. Twin circle property

Now we generalize the arbelos. Let α and β be circles with diameters OA and OB as before, and γ an arbitrary circle or a line touching α and β at points different from O . There are two areas surrounded by the three circles and we select one of the area in the following way (Figure 16): If γ touches α and β externally from above, we choose the finite area, if γ touches α and β internally, we choose the upper area, and if γ touches α and β externally from below, we choose the infinite area. We call this area the skewed arbelos formed by α , β and γ . Now we define four chains of circles, where some circles may be a line parallel to the y -axis. There are two circles touching α , γ and the y -axis which do not pass through O , and label the one inside the skewed arbelos as α_0^+ and the other one as α_0^- . There are also two circles touching α , α_0^+ and the y -axis, one intersecting γ and the other not. We label the former as α_{-1}^+ and the latter as α_1^+ . The circles α_2^+ , α_3^+ , \dots can be defined inductively in the following way: Assuming the circles α_{i-1}^+ and

α_i^+ are defined, α_{i+1}^+ is the circle touching α , α_i^+ and the y -axis and different from α_{i-1}^+ . The circles α_{-2}^+ , α_{-3}^+ , \dots are defined similarly. Now the entire chain of circles

$$\{\dots, \alpha_{-2}^+, \alpha_{-1}^+, \alpha_0^+, \alpha_1^+, \alpha_2^+, \dots\}$$

is defined. The other three chains of circles

$$\{\dots, \alpha_{-2}^-, \alpha_{-1}^-, \alpha_0^-, \alpha_1^-, \alpha_2^-, \dots\},$$

$$\{\dots, \beta_{-2}^+, \beta_{-1}^+, \beta_0^+, \beta_1^+, \beta_2^+, \dots\},$$

$$\{\dots, \beta_{-2}^-, \beta_{-1}^-, \beta_0^-, \beta_1^-, \beta_2^-, \dots\},$$

where α_{-1}^- , β_{-1}^+ and β_{-1}^- intersect γ , are defined similarly (Figure 17).

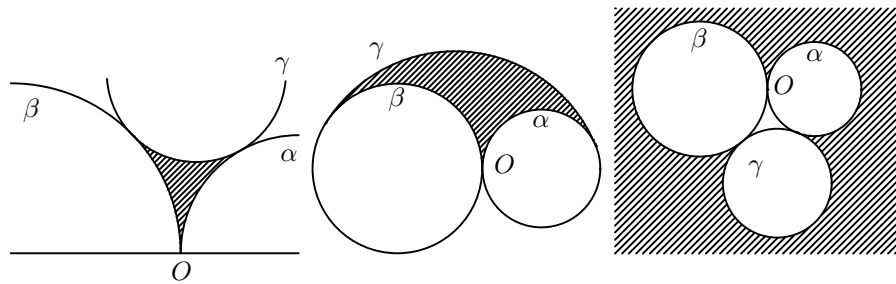


Figure 16

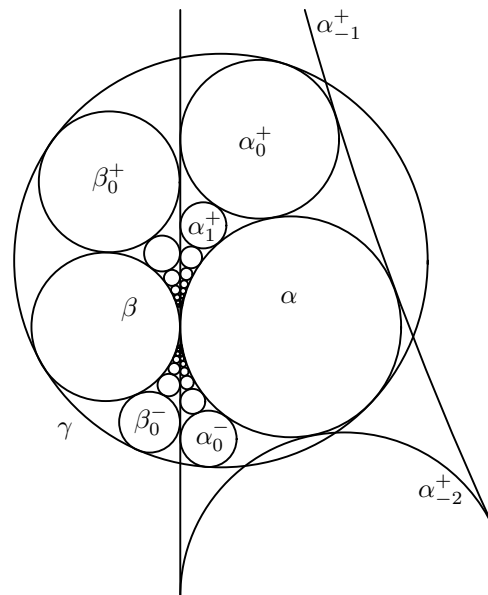


Figure 17

The circle γ always passes through points $(0, 2\sqrt{ab}/(z \pm 1))$ for a real number z . There are a dozen of twin circles in the skewed arbelos under

certain conditions. One of the most notable ones are as the following, which are generalizations of the twin circles of Archimedes [5].

Theorem 7. *Let n be an integer. Each of the pairs of the circles α_n^+, β_n^+ ; $\alpha_{-n}^-, \beta_{-n}^-$; α_{-n}^+, β_n^- ; α_n^-, β_{-n}^+ are congruent if and only if γ passes through the points $(0, 2\sqrt{ab}/(n \pm 1))$.*

The circle γ is one of the tangents in the case $n = \pm 1$, and the twin circles of Archimedes is obtained when $n = 0$.

3. Geometric animation

There are several Internet sites where Java applets on the arbelos can be seen, most of which are demonstrating very simple properties. Thomas Schoch's site is one of the most comprehensive among of them, where several Java animations on some of the results in [3] can be found [12].

Some of our generalizations of the arbelos show properties that a circle with fixed size always appears for a certain condition when other geometric elements vary. In Theorem 1, the size of the inscribed circle is constant for variable m and n satisfying (1). In Theorem 3, the size of the circle passing through O is also constant when the point of intersection of the tangents on α varies. Those properties can easily be seen at a glance if there are geometric animations to demonstrate them. This is the reason that we thought of making geometric animation programs on the arbelos. We were faculty members in a department of information engineering at that time (in 2006), and used the generalizations of this figure in computer education. We gave several problems to make Java programs on generalizations of the arbelos to a group of senior students. After learning a brief introduction of Java language for two months (they already knew C programming language), they turned to writing programs.

But all the student tried to make programs in the easiest way, which resulted in non smooth animations, sometimes very quick and sometimes very slow motions. We had to give suggestions to choose parameters carefully so that the motion of the animations would be smooth and constant. The most important thing is to consider which geometric element should be chosen to animate the figure. For example, for the animation of Figure 7, a student chose the radius of the circle $\alpha(m)$ as a varying parameter to animate the figure. The result was very slow motion when the size of $\alpha(m)$ was very large. A right way should be to change the angle determined by the line AB

and the line joining the centers of γ and the inscribed Archimedean circle constantly. Some of our applets can also be seen at Schoch's site [12].

It is said that Java language has a feature that the programs can be "run anywhere". But we now realized a couple of other advantages of this for geometric animation: no need to pay licence fee, no need of special graphic package, easy use for web based presentation and existence of a huge amount of informations about this language in the Internet.

4. An example of history and development of mathematics

From an educational point of view, it would be very effective for the students if they could see concrete examples how each of the theories developed step-by-step. There are many books of history and development of mathematics. But it is rather difficult to see such developments in those history books, because they only give a broad overview and do not discuss each of the theories precisely. This means that it is not easy for students at the undergraduate level to see a concrete example how each of the theories developed unless they read some research papers sequentially, but it is almost impossible.

On the other hand, recent developments of the arbelos offer several comprehensible concrete examples of developments of mathematics, which can be understood even by high school students, since we can explain using figures. Indeed several articles on recent developments of the arbelos were published not in a mathematics journal but in a monthly science journal in Japan [10]. Moreover the geometric animation can be of some help for their understanding. Masayuki Watanabe gave a lecture entitled "The arbelos, past, present and the futures" to citizens in our city Maebashi using those animations [13].

5. Conclusion

The arbelos has often been used in mathematics education especially in problem solving. But recent generalizations enables further uses of this figure. They give good geometric computer animation materials, which are useful for education of computer graphics and computer programming. The generalizations also gives concrete examples of developments of mathematics, which are comprehensible to even high school students. The animations can be very useful for their understanding.

References

- [1] Bankoff, L. (1974). Are the twin circles of Archimedes really twins? *Math. Mag.*, **47** 134-137.
- [2] Bankoff, L. (1994). The marvelous arbelos, in *The lighter side of mathematics* 247-253, ed. R. K. Guy and R. E. Woodrow, Mathematical Association of America.
- [3] Dodge, C. W., Schoch, T., Woo, P. Y. and Yiu, P. (1999). Those ubiquitous Archimedean circles, *Math. Mag.*, **72** 202-213.
- [4] Okumura, H. and Watanabe, M. (2004). The Archimedean circles of Schoch and Woo, *Forum Geom.*, **4** 27-34.
- [5] Okumura, H. and Watanabe, M. (2004). The twin circles of Archimedes in a skewed arbelos, *Forum Geom.*, **4** 229-251.
- [6] Okumura, H. and Watanabe, M. (2005). The arbelos in n -aliquot parts, *Forum Geom.*, **5** 37-45.
- [7] Okumura, H. and Watanabe, M. (2006). A generalization of Power's Archimedean circles, *Forum Geom.*, **5** 103-105.
- [8] Okumura, H. and Watanabe, M. (2007). Characterizations of an infinite set of Archimedean circles, *Forum Geom.*, **7** 121-123.
- [9] Okumura, H. and Watanabe, M. (2007). Remarks on Woo's Archimedean circles, *Forum Geom.*, **7**, 125-128.
- [10] Okumura, H. and Watanabe, M., Gifts from Archimedes, *Kagaku*, **75** number 6 (2005) 746-749, **75** number 11 (2005) 1314-1318, **76** number 4 (2006) 406-409, **76** number 10 (2006) 1053-1055, **77** number 9 (2007) 992-993, Iwanami Shoten (in Japanese).
- [11] Power, F. (2005). Some more Archimedean circles in the arbelos, *Forum Geom.*, **5** 133-134.
- [12] Schoch, T., <http://www.retas.de/thomas/arbelos/arbelos.html>.
- [13] Watanabe, M. (2006). The arbelos, past, present and the futures, <http://www.maebashi-it.ac.jp/library/chiken/H18-koukaikouza.pdf>.

A \LaTeX plotting software *KETpic* and its development

Yuuki TADOKORO Takayuki ABE Kenji FUKAZAWA
Masataka KANEKO Masayoshi SEKIGUCHI Satoshi YAMASHITA
Setsuo TAKATO*

tado@nebula.n.kisarazu.ac.jp

Natural Science Education

Kisarazu National College of Technology

Japan

Abstract

We have developed a \LaTeX plotting software and call it *KETpic*. It is a macro package for Maple [5] and Mathematica [6], which are famous computer algebra systems (CASs). *KETpic* enables us to draw fine pictures in \LaTeX documents. It is useful particularly for typesetting mathematical documents. In this paper, we explain properties, advantages and perspectives of *KETpic* with its examples.

1 Introduction

Mathematics teachers, mathematicians, and many scientists need illustration tools for their education and research. Many people of them utilize \LaTeX documents. However, it is not easy to embed clear and well-arranged figures into the documents. We can include picture files, for example, Encapsulated PostScript (EPS) files into the documents. In order to prepare these files, we need softwares: Gnuplot, Adobe Illustrator, and so on. They are not always good for typesetting mathematical documents, because EPS files are not easy to be improved. Furthermore, their file size is large in general. We give one solution, *KETpic*.

In order to write mathematical textbooks using \LaTeX , we started developing a Maple macro package *KETpic* [2]. Recently we have developed *KETpic* for Mathematica. After loading *KETpic* as a macro package, Maple and Mathematica can generate a text file which consists of Tpic specials codes from graphical plotdata. Here, plotdata are internal expressions for a CAS, which can be manipulated like any other expression of the CAS. We can input these codes as commands of the picture environment in \LaTeX source files by the command `\input`. Tpic is a graphic extension of \TeX which uses a simpler set of embedded commands [1]. Basically, the outputs are independent of DVI drivers and

*The Toho University

easy to be improved from the help with CASs. Since their file is a text one, its size is sufficiently small to be handled. Also the figures are fine and clear. Therefore, they are suitable for mathematical typesetting and research. In this paper we explain how to use KETpic with its beautiful examples, benefits and perspectives.

2 Properties and Advantages of KETpic

We introduce how to make Figure 1, in the case of a Windows PC which we install KETpic for Mathematica on. We explain how to use KETpic and some advantages of it.

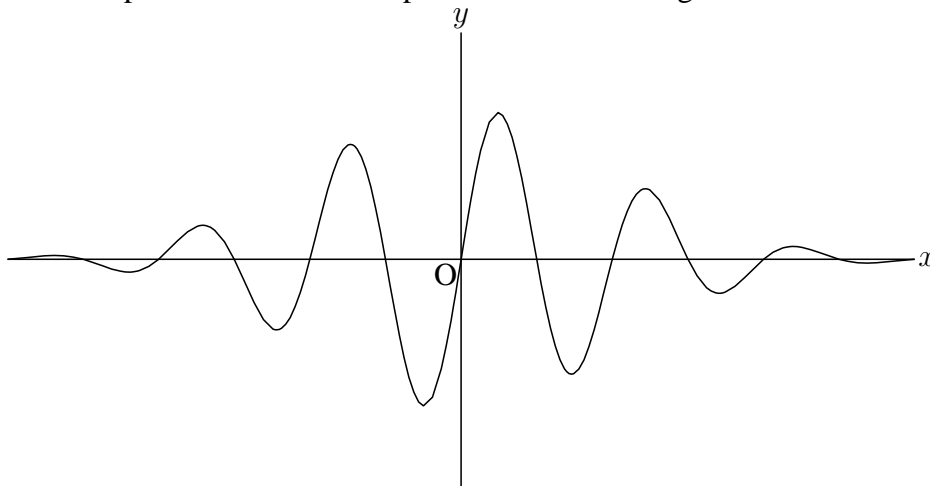


Figure 1: An example

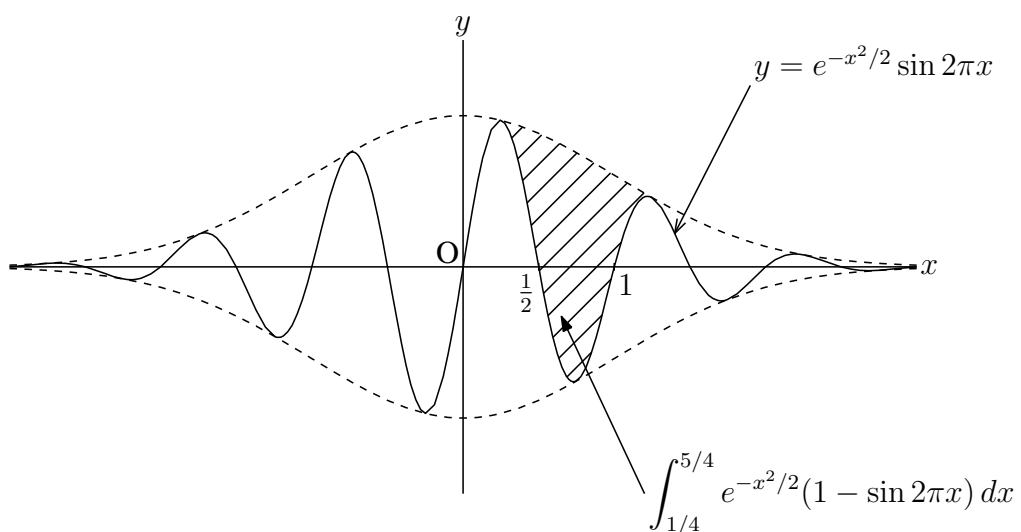


Figure 2: Figure 1 with accessories

1. We download ketpicmath6.m to a folder, for example, C:\Work from Web site [4]. It is a KETpic for Mathematica.

2. Using Mathematica with KETpic, we make a \LaTeX file including plotdata and graph accessories.

(a) Load KETpic.

```
<< C:\\Work/ketpicmath6.m
```

We remark that the double backslash “\\” returns a single backslash because it is a control code in Mathematica.

(b) Specify the window size and produce the plotdata of functions.

```
setwindow[{-3,3},{-1.5,1.5}];
(* specify the window size *)
g1=plotdata[Exp[-x^2/2]*Sin[2*Pi*x],{x,XMIN,XMAX}];
(* generate the plotdata without displaying *)
windisp[g1] (* optional: display the plotdata *)
```

(c) Open a \LaTeX file and write plotdata into it. Here we call it f1.tex

```
openfile["C:\\Work/f1.tex"]
(* open a file in a folder *)
openpicture["1cm"]; (* start the picture environment *)
drwline[g1]; (* write down the plotdata *)
closepicture[0]; (* finish the picture environment *)
closefile[] (* close the file *)
```

3. Insert the \LaTeX file f1.tex into the user’s \LaTeX source file.

```
\documentclass[a4paper]{article}
\newlength{\Width} %
\newlength{\Height} % the length parameters of KETpic
\newlength{\Depth} %
\begin{document}
\input{f1.tex}
\end{document}
```

After the usual compilation of this \LaTeX file, we obtain Figure 1.

Plain CASs can embed clear figures into \LaTeX documents as an EPS file. The quality, however, is not satisfactory. For example, the font in the picture is different from one in documents and it is not so easy to improve the picture. CASs with KETpic enable us to use the same font embedded in \LaTeX documents and improve the pictures. In Figure 2, we attach accessories to Figure 1: dashlines, hatched lines, arrows, and writing mathematical expressions. Moreover, we modify the width of the gap and thickness of lines. We can use other accessories, for examples, thick lines, bow data, setting axes, tick marks, etc. See Figure 3, 4.

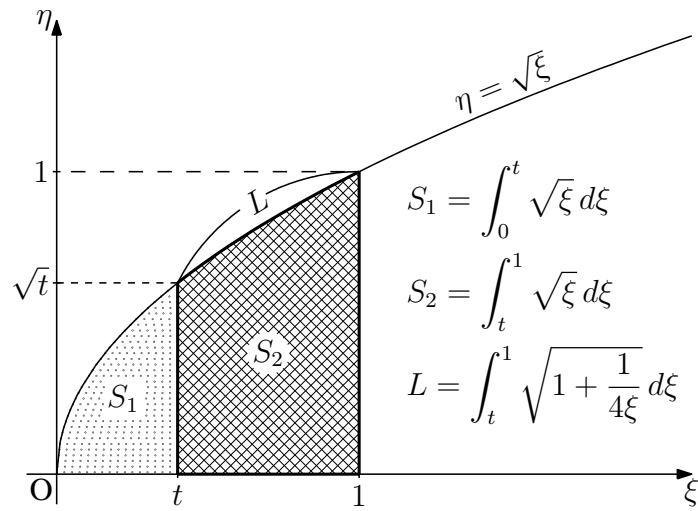


Figure 3: An example with accessories

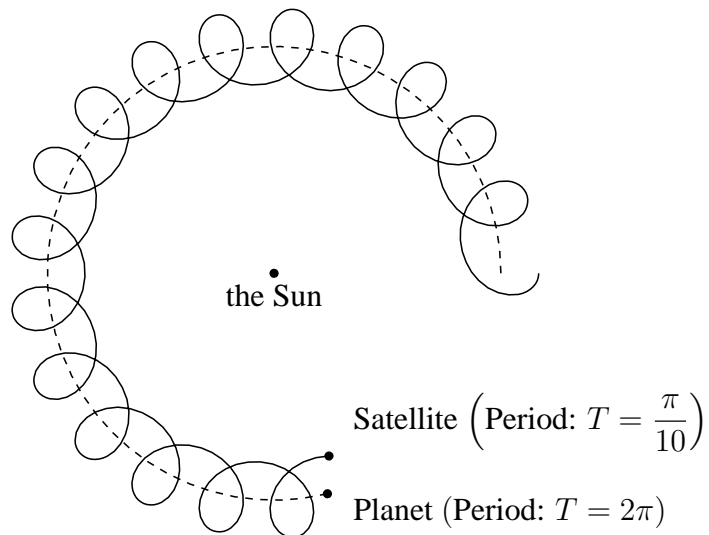


Figure 4: An orbit of a retrograde satellite with its mother planetary orbit

We give examples, Figure 5 and 6. You might think CASs provide higher accuracy numerical data. We use the programming of them and show partially the source of Figure 6 in Maple as below. We need reading the Maple package, `> with(plottools):`.

```
> setwindow(-4..4,-3..3):
> C:=t->circle([t,0],sqrt(t^2/5+1/4)):
> tmp:={C(0)}:
  t:=0:
  for i from -4 by 0.5 to 4 do
    tmp:=tmp union C(i):
  od:
> E:=display(op(tmp)):
> h1:=plot([sinh(s),cosh(s)/2,s=-3..3]):
> h2:=plot([sinh(s),-cosh(s)/2,s=-3..3]):
> windisp(E,h1,h2);
```

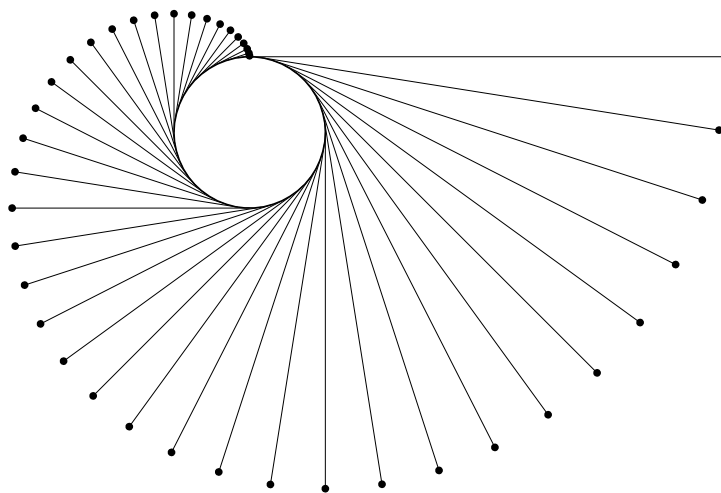


Figure 5: An involute of a circle

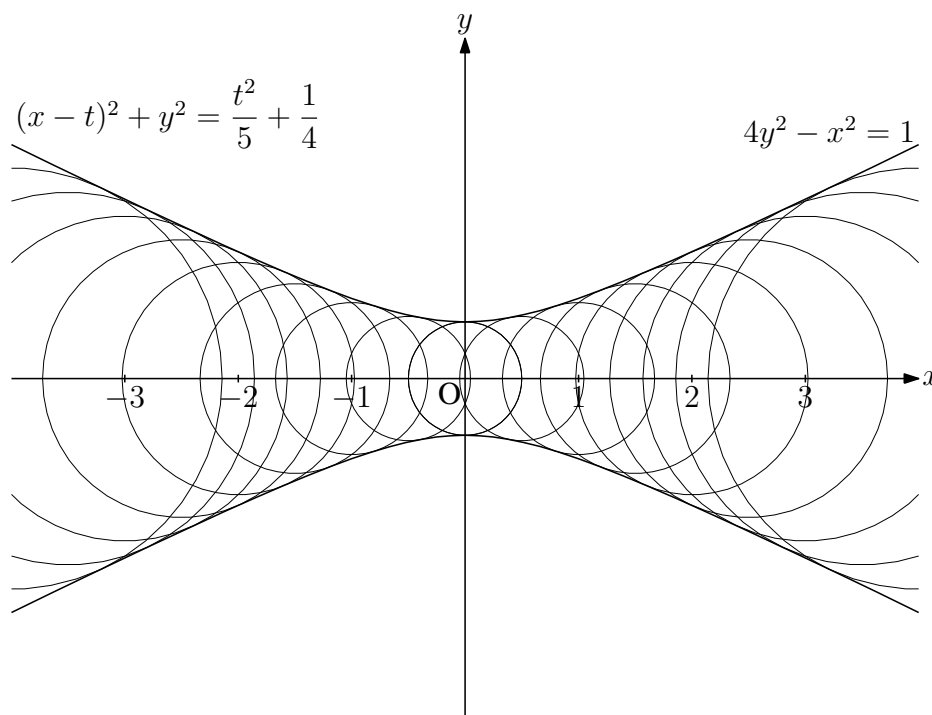


Figure 6: An envelope of a set of circles

Easy improvement (attaching many accessories) and CASs' higher accuracy are important advantages of KETpic. Others are availability for famous CASs: Mathematica and Maple. It is also available for major operating systems: Windows, Macintosh, and Linux. KETpic is a free software and downloadable from [4]. KETpic does not supports a color package so far. But, we think the monochrome (low cost) printed matter is suitable for mathematics class.

We have been developing to handle 3D graphics. We show available functions: the parallel projection, the perspective projection, and the skeleton view. In the parallel projection, we specify a view direction. The skeleton view function in this projection grabs the height data by hiding distant curves. We show such examples about the regular dodecahedron. We obtain two pictures in Figure 7 derived from almost the same programs. The unique difference is the view direction. On the other hand, we specify a viewpoint in the perspective projection. By changing the viewpoint, we can make stereograms easily. Figure 8 realizes a 3D image in our brain by a cross-eyed view, that is, looking at the left picture with the right eye and vice versa. See [2] or [4] for example.

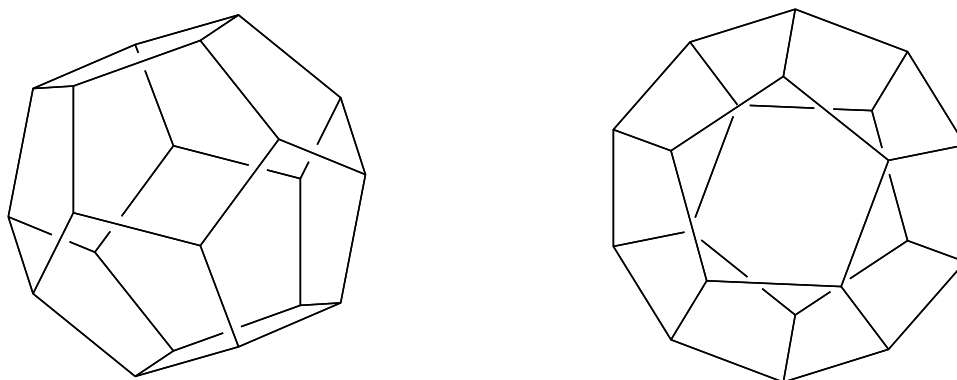


Figure 7: The regular dodecahedron from two different view directions

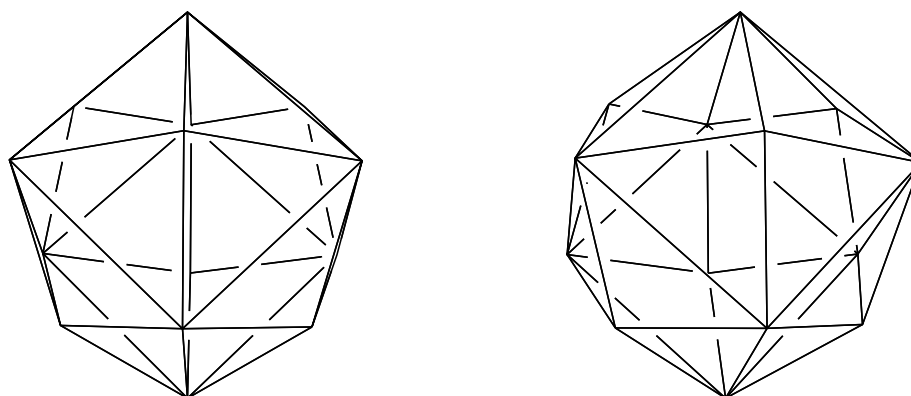


Figure 8: A stereogram of the tetrakisshexahedron

3 KETpic for Maple versus Mathematica

We show the program of KETpic for *Maple* making Figure 1. Then you might guess two KETpics of Mathematica and Maple seem to be essentially same in some sense.

```
> with(plots):
> read `C:\\Work/ketpicw.m`:
> setwindow(-3..3,-1.5..1.5):
> g1:=plot(exp(-x^2/2)*sin(2*Pi*x), x=XMIN..XMAX):
> windisp(g1);
> openfile(`C:\\Work/fl.tex`):
> openpicture("lcm"):
> drwline(g1):
> closepicture(0):
> closefile():
```

We remark that `> with(plots):` means reading the package which is proper to Maple. Almost differences of KETpic for Mathematica and Maple are their original commands.

4 Summary and Perspective

KETpic is a macro package of CASs to generate Tpic specials codes. It enables us to draw clear and fine pictures in \LaTeX documents. The current applicable CASs are Mathematica and Maple. Its advantages are easy improvement, higher accuracy, and availability for major operating systems. KETpic is very useful for typesetting mathematical documents and research. However, it is not sufficient for 3D graphics and available for free CASs. We will equip KETpic with the feature of 3D surfaces, and extend KETpic to other free CASs, such as Maxima and Scilab.

References

- [1] M. Goossens, S. Rahtz, and F. Mittelbach: *The \LaTeX Graphics Companion: Illustrating Documents With Tex and Postscript*. Addison-Wesley, 1997.
- [2] M. Sekiguchi, S. Yamashita, and S. Takato: *Development of a Maple Macro Package Suitable for Drawing Fine \TeX -Pictures*. Lecture Notes in Computer Science **4151**, 24-34, Springer-Verlag, 2006.
- [3] M. Sekiguchi, M. Kaneko, Y. Tadokoro, S. Yamashita, and S. Takato: *A New Application of CASs to \LaTeX Plottings*. Lecture Notes in Computer Science **4488**, 178-185, Springer-Verlag, 2007.
- [4] M. Sekiguchi: <http://www.kisarazu.ac.jp/~masa/math/E.html>

- [5] M.B. Monagan, K.O. Geddes, K.M. Heal, G. Labahn, S.M. Vorkoetter, J. McCarron, and P. DeMarco: *Maple 10 Advanced Programming Guide*. Maplesoft, Waterloo, Ontario, Canada, 2005.
- [6] Wolfram, Stephen: *The Mathematica book, Fifth Edition*. Wolfram Media/Cambridge University Press, 2003.

On Proof Techniques and Technology

Ma. Louise Antonette N. De Las Peñas

mlp@mathsci.math.admu.edu.ph

Department of Mathematics
Ateneo de Manila University
Philippines

Debbie Marie Y. Bautista

debbie@mathsci.math.admu.edu.ph

Department of Mathematics
Ateneo de Manila University
Philippines

Abstract: In this paper, we discuss ways on how technology enables students to investigate mathematical ideas, discover facts and formulate good proofs.

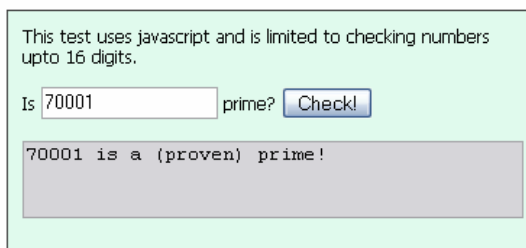
1. Introduction

Proofs form an integral part of mathematical knowledge and are springboards for the development of new mathematical theories. One of the challenges that confront mathematics students is being able to understand and write good mathematical proofs. Students who have an in-depth understanding of the mathematical concepts will most likely be able to write correct proofs. Creating proofs is an art that improves with practice. Technology has the power of being able to engage the learner in explorations leading to conjecture and to experience what it means to construct knowledge (Rivera, 2005). Students become more motivated when they are able to construct figures in solving proof-problems. Writing a proof includes a clear statement of the conjecture, which allows for the connection between the hypothesis and the conclusion. Technology allows for experimentation with diagrams and tables to see how parts of the hypothesis are related. Dynamic geometry, for example, facilitates with ease what happens to properties of geometric objects when being moved around the plane. Moreover, technology provides a means to apply the various rules of logic that are strategies to determine the validity of one's conjectures. In this paper, situations which reflect the role of technology in the construction of mathematical proofs are highlighted.

2. Examples and Counterexamples in Proofs

We first consider an example taken from Foster (1999). Consider the expression $n^2 - n + 41$ for any natural number n . A spreadsheet could easily show that the first few values are 41, 43, 47, 53, and 61 (Figure 1(a)). Students can conjecture that this expression is prime for all natural numbers. To test the conjecture, one may check larger values of n such as 265. For this value of n , the expression yields 70001. To determine whether this is prime, one may use primality tests available over the web, such as in [11]. (See Figure 1(b)).

n	$n^2 + n - 41$
1	41
2	43
3	47
4	53
5	61
6	71
7	83
8	97
9	113



(a)

(b)

Figure 1: Investigating the expression $n^2 - n + 41$

However, it is evident that the conjecture fails for $n = 41$. This is an example which shows that a proof based on examples, no matter how many, is not considered valid. It also shows that one counterexample is sufficient to disprove a conjecture. Technology facilitates the investigation of this conjecture since it allows students to easily evaluate an expression and check primality. Since students do not need to perform tedious computations, they can focus on the main problem.

3. Verifying the Converse and Contrapositive

Dynamic geometry can facilitate the investigation of a statement and its converse. In this example, we use the free dynamic mathematics software Geogebra (Hohenwarter, 2001). In Figure 2, students may drag the chords of the circle and check whether two congruent chords could have different distances from the center of the circle. Similarly, they can drag the chords to examine whether chords equidistant from the center of the circle could have different lengths.

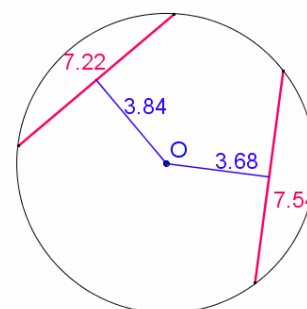


Figure 2: Exploring Chords in a circle

A less common example is Desargues' theorem in Projective Geometry: *In the real projective plane, if two triangles are perspective from a line, then they are perspective from a point.* Explorations through the Geometer's Sketchpad allow the students to verify that if triangles are perspective from a point, an axis of perspectivity may be obtained as well! They discover that the converse holds, and the theorem and its converse together state that the two notions of perspectivity are equivalent. Figure 3 shows that the black triangles are perspective from point A if and only they are perspective from the line containing X, Y and Z. On the other hand, the gray triangles are perspective from the point X and also perspective from the line containing A and the left vertices of the black triangles.

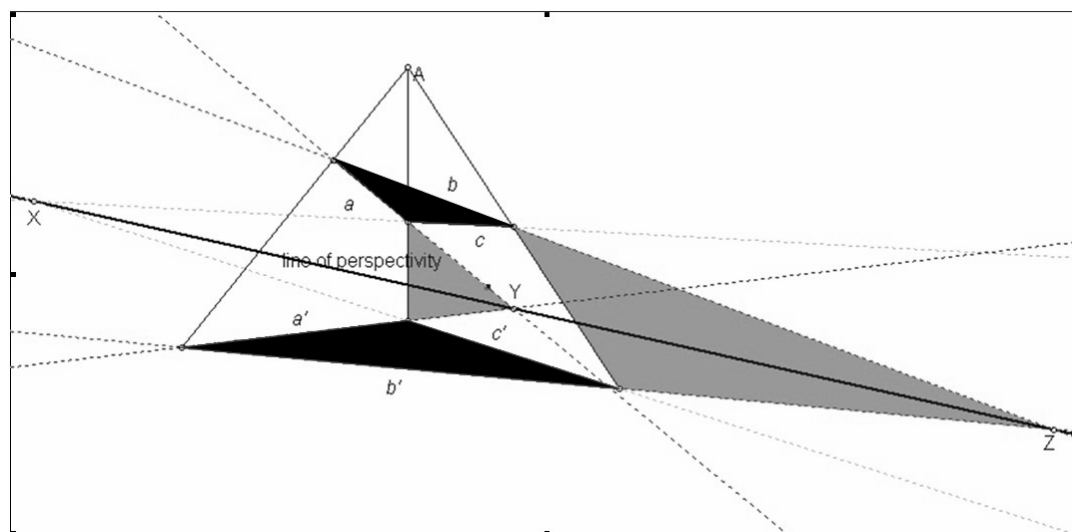


Figure 3: Investigating perspectivity from the point and line

Dynamic geometry software such as Geogebra can also verify the validity of a mathematical statement through its contrapositive form. This will be demonstrated through one variation of the Steiner-Lehmus Theorem. Recall that in $\triangle ABC$, if the bisector of the exterior angle $\angle ABH$ meets side \overline{AC} extended at point G , then the line segment \overline{BG} is called the angle bisector at B (see Figure 4a). The theorem states that *if a triangle is isosceles, then two of its external bisectors are congruent*. To discover this, students may drag point B anywhere on the circle and note that the triangle ABC remains isosceles. By dragging B , students determine whether it is possible for the two external bisectors to have unequal lengths and discover that it cannot be done. Whenever points B and C lie on circle A , the two external bisectors shown are congruent. To further verify this conjecture, students investigate the contrapositive: if the two exterior bisectors shown are not congruent, can the triangle be isosceles (see Figure 4b)? Students may then form their conjectures based on their observations. Finally, they could explore whether the converse holds. If two of the external bisectors of a triangle are congruent, can the triangle be isosceles? Or in its contrapositive form: if a triangle is not isosceles, then will two of its external bisectors be not congruent? They should then discover that this is not so (see Figure 4c). In using these types of activities, though, one should be careful to understand that the activity serves not as a proof by itself. Usually, when using the measurement tool in a dynamic geometry environment, measurements are not exact, but numeric in nature. As such, these values are subject to rounding errors and what appears to be equal may be not so. Rather, these activities act as a springboard to pursue the idea further and prove one's conjectures.

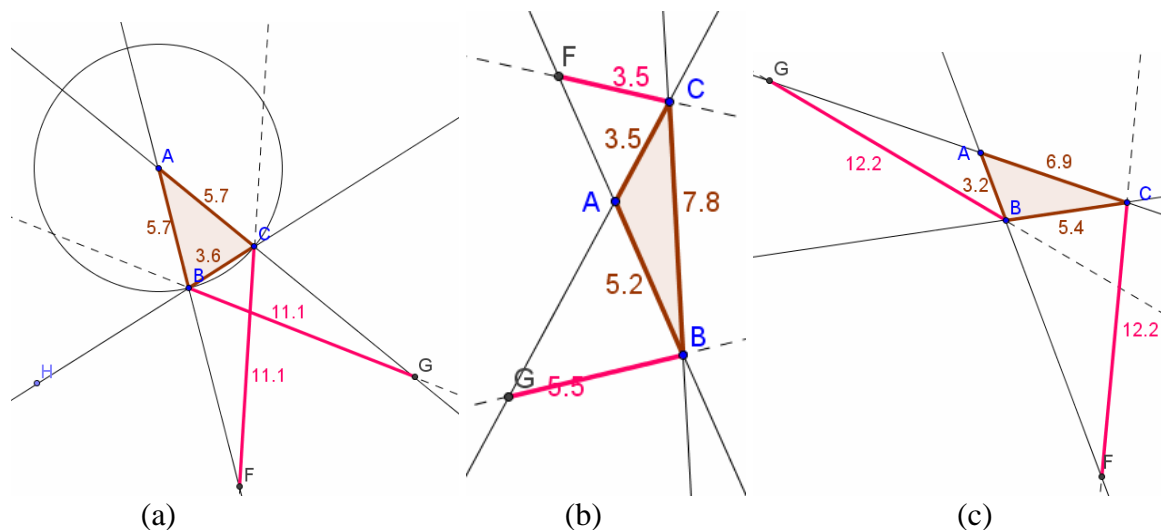


Figure 4: Investigating the exterior bisectors of a triangle

4. Explaining Patterns and Relationships

An interesting result occurs when 37 is multiplied to the first nine multiples of 3 (Posamentier, 1999). Let students discover this by using a calculator or spreadsheet (See Figure 5).

n	$37 \times n$
3	111
6	222
9	333
12	444
15	555
18	666
21	777
24	888
27	999

Figure 5: Studying interesting number patterns

Help students realize that by knowing that $37 \times 3 = 111$, then the rest of the results would follow. To further extend this idea, have them multiply 12345679 by the first 9 multiples of 9. This yields the table in Figure 6.

n	$12345679 \times n$
9	111111111
18	222222222
27	333333333
36	444444444
45	555555555
54	666666666
63	777777777
72	888888888
81	999999999

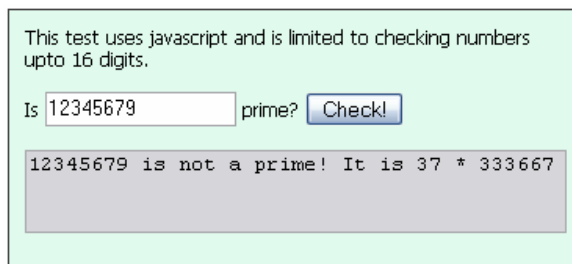


Figure 6: Investigating Number Patterns

What about the number 12345679 gives these results? Technology allows students to explain the remarkable number patterns. One may use [11] to determine two numbers whose product is 12345679 (see Figure 6). This test reveals that 12345679 is 37 times 333667. Now, what about the number 333667 could explain the number patterns? From the previous exercise, it was observed that $37 \times 3 = 111$. What is 333667×3 ? Combining these facts, students should be able to explain why $9 \times 12345679 = 111111111$.

In the previous example, technology is used in two ways: to discover interesting number patterns and to explain why such patterns exist. The tools allowed students to determine factors of large numbers easily so that they could focus on the proof itself.

As a second illustration, we present color models generated by the abstract algebra feature of *Mathematica* (see Figure 7). These models allow students to study patterns in and relationships of group structures. Students often find the underlying concepts governing the structure and properties of groups difficult to grasp, with the proofs involving a high level of abstraction. For instance, Figures 7(a), (b) and (c) show respectively, the group tables of $Z_8/\{0,4\}$, Klein 4 group and Z_4 . Through the models the students can explore the relationships of the group structures, and conclude the isomorphic relationship of $Z_8/\{0,4\}$ and Z_4 . Moreover, students may be asked to verify properties of left cosets for abelian groups: in Figure (a) for instance, is left coset multiplication well-defined?

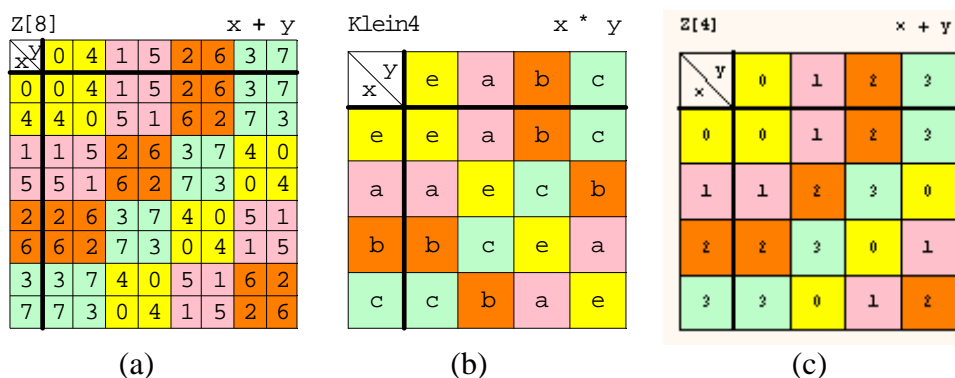


Figure 7: Studying Group Relationships

5. Mathematical Induction

Some results that can be proved using mathematical induction can be introduced using technology. For this example, we use Cuisenaire rods. This problem was taken from Count the Trains [1]. The problem is to determine how many trains of length n can be constructed using cars which are either 1 or 2 units long. The following configuration is an example for $n = 12$. The mirror image of this train is counted differently.

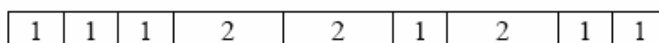


Figure 8: Investigating Number Patterns

Students first investigate the answer for $n = 1, 2, 3,$ and 4 using Cuisenaire rods. They are then asked to tally their results in a table and find a pattern. Upon completing the results for small values of n , students are able to observe that their results are the consecutive elements of the

Fibonacci sequence. This can then be taken as a starting point for proving by mathematical induction.

6. Existence, Uniqueness, and Impossibility Theorems

Dynamic geometry software such as Geogebra facilitates investigations on existence and uniqueness. For instance, consider Figure 9.

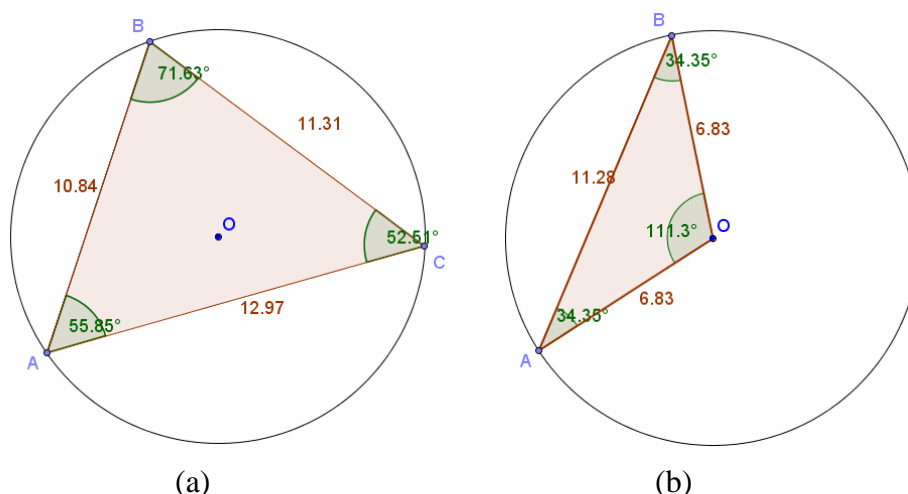


Figure 9: Exploring triangles in relation to a circle

In Figure 9a, students could drag vertices A , B , or C to determine whether any of the following triangles can be constructed with A , B and C on the circle: Equilateral, Acute Isosceles, Right Isosceles, Obtuse Isosceles, Acute Scalene, Right Scalene, Obtuse Scalene. A similar exercise could be done when two of the vertices of the triangle lie on the circle while the third vertex is on the center of the circle (See Figure 9b). Students could first explore triangles which can be formed, and triangles which are impossible to construct under these conditions. To maximize the benefit of this activity, students should be asked to explain why some triangles cannot be formed under the given conditions.

Another example may be carried out through the free dynamic geometry software *Non-Euclid* (Castellanos et al, 1994) or through Geometer's Sketchpad. Here, students can first explore the impossibility of Euclid's 5th Postulate and Playfair's Axiom in the Poincare' model of the hyperbolic plane. Euclid's Postulate: *If two lines are intersected by a transversal such that the sum of the degree measures of the interior angles on one side of a transversal is less than two right angles then the lines meet on that side of the transversal* and Playfair's Axiom: *Given a line l and a point P not on the line, there is exactly one line through P parallel to l* are equivalent conditions for parallelism in the Euclidean plane. Students may be asked to show why in the hyperbolic plane, there are at least two lines through P parallel to l .

In Figure 10, there are two lines through C parallel to line DB . Point G cannot be on HC , for if it were, then $GCDB$ would be a rectangle. The measurement menu shows HC and CG parallel to DB .

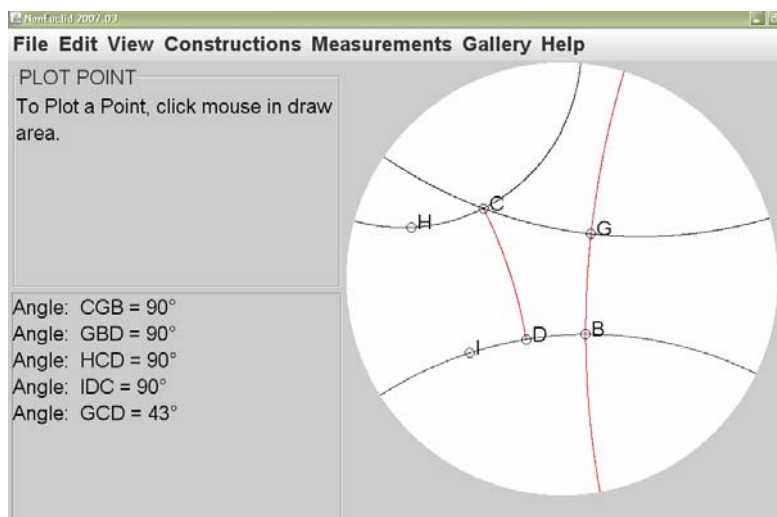


Figure 10: Probing Euclid’s postulate

7. Coordinate Geometry

The use of coordinate geometry in proofs connects geometric and algebraic ideas. A great benefit of technology is being able to facilitate the development of a proof using coordinate geometry. Consider the Nine-Point Circle Theorem which states that *in any triangle, the midpoints of the three sides, the feet of the three altitudes, and the midpoints of the segments joining the three vertices to the orthocenter all lie on a circle* (see Figure 11a).

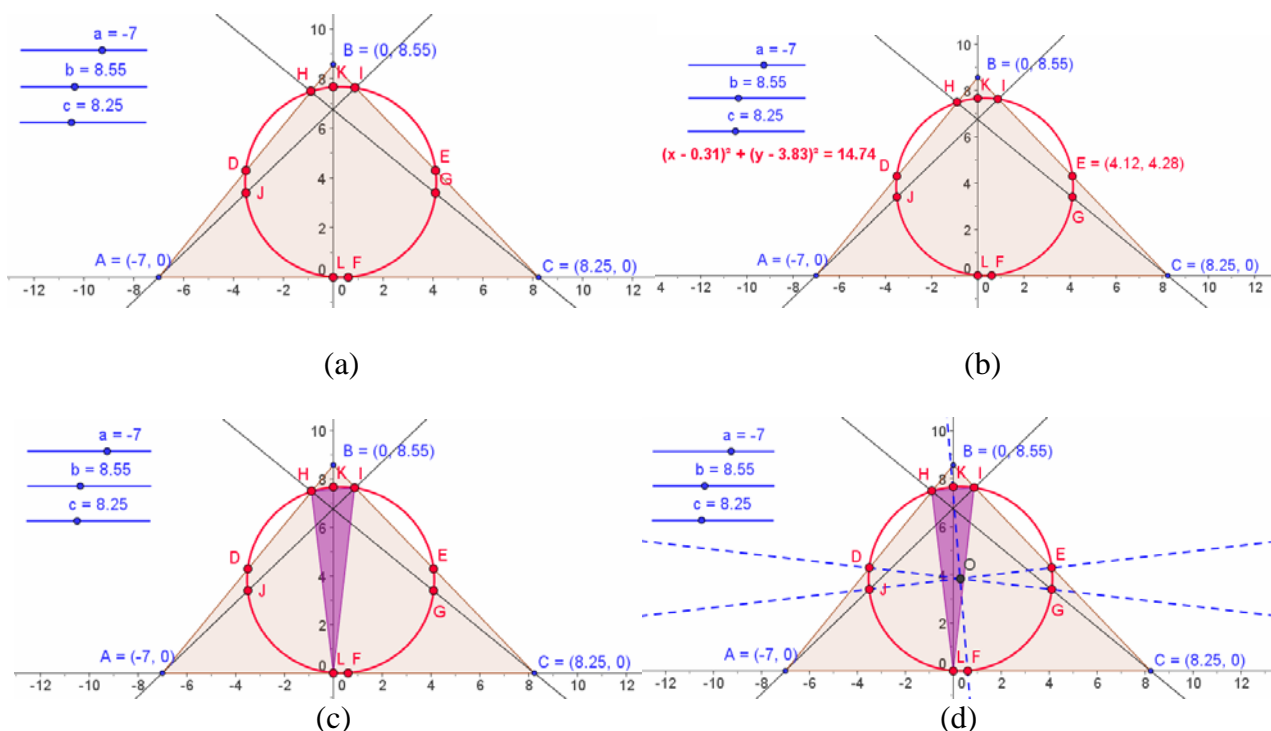


Figure 11: The nine-point circle

Students may use dynamic geometry to discover or to verify that the nine points indeed lie on the circle. Further, students may use this technology to display the equation of the circle and to show the coordinates of any point. In Figure 11b, the coordinates of Point E is shown along with the equation of the nine-point circle. Students may then verify using coordinates whether the point lies on the circle by plugging in values.

One way of proving this is axiomatic in nature. Another way is analytic and can be found in Reynolds & Fenton (2006). The analytic proof involves complicated computations, and this is where technology might come in. By using a computer algebra system (CAS) such as Scientific Workplace, routine calculations can be done with ease so that students could focus on the proving technique. For instance, to find the coordinates of H , after typing a system of linear equations, one may click on the Solve tool  of Scientific Workplace to solve the system (see Figure 12).

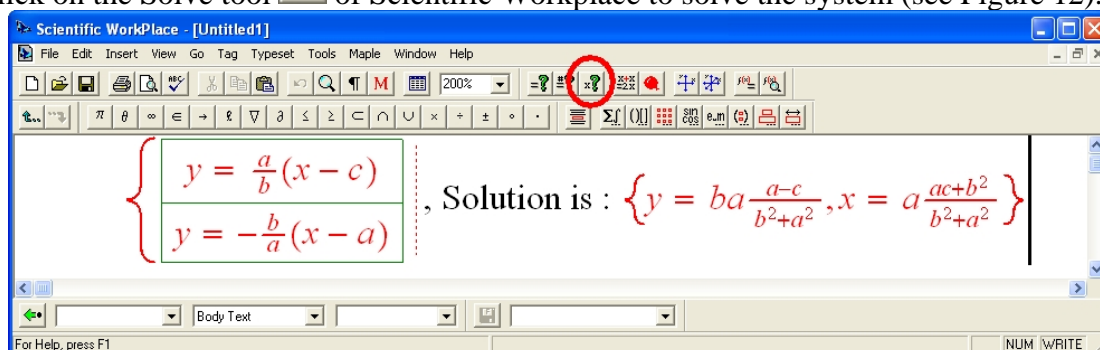


Figure 12: Using CAS to solve a system of equations

Further in the proof, one makes use of the triangle formed from the three feet of the altitudes of $\triangle ABC$, as shown in Figure 11c. One needs to derive the perpendicular bisector each side of this triangle. To illustrate, we will use CAS to find the equation of the perpendicular bisector of \overline{HL} . Using the point H above and $L(0, 0)$, one can use the Simplify tool  of Scientific Workplace to find an expression for the slope:

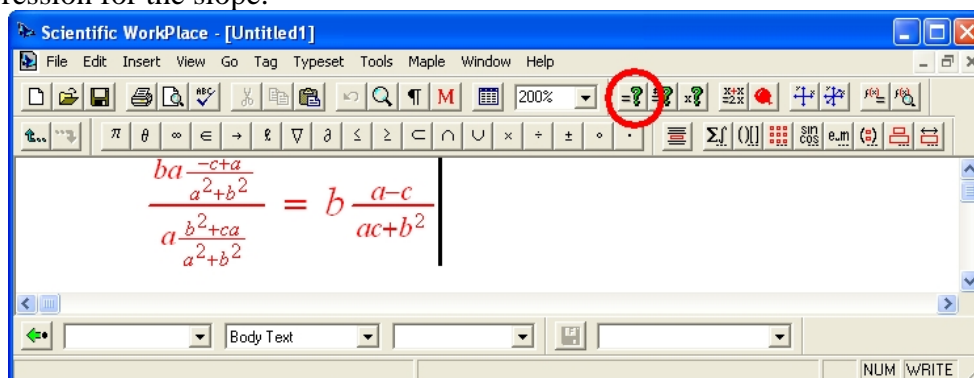


Figure 13: Using CAS to simplify expressions

From here, one can again use the Simplify tool  to obtain the equation of the perpendicular bisector of \overline{HL} .

$$y = -\frac{1}{b} \frac{b^2+ca}{-c+a} \left(x - a \frac{b^2+ca}{a^2+b^2} \right) + ba \frac{-c+a}{a^2+b^2} = \frac{-xb^2+ab^2+ac^2-cax}{b(-c+a)}$$

Figure 14: Using CAS to obtain the equation of the perpendicular bisector of \overline{HL}

The same steps are repeated to find the equation of perpendicular bisectors of \overline{HI} and \overline{IF} (see Figure 11d). Finally, one can use the Solve tool  to obtain the intersection of two of the perpendicular bisectors to obtain the coordinates of the center O of the circle.

$$\left\{ \begin{array}{l} y = \frac{-(b^2+ac)}{b(a-c)}x + \frac{a(b^2+c^2)}{2b(a-c)} \\ y = \frac{-(b^2+ac)}{b(c-a)}x + \frac{c(a^2+b^2)}{2b(c-a)} \end{array} \right. , \text{ Solution is : } \left\{ x = \frac{1}{4}c + \frac{1}{4}a, y = \frac{1}{4} \frac{-ac+b^2}{b} \right\}$$

Figure 15: Using CAS to obtain the center of the circle

One can then see that the coordinates of the center of the nine-point circle is completely determined by the values of a , b , and c . Indeed, one can use the values of a , b , and c in Figure 11b to find the center of the circle and see that it agrees with the equation of the circle shown.

7. Finding solutions to open problems

Proving with the aid of technology is not merely a means of verifying an already discovered result, but also a means of exploring, analyzing, discovering and inventing new results. For example, technology can bring forward the transformational approaches to discovering interesting properties of mathematical groups in the hyperbolic plane. In Figure 16 we show Dunham’s computer modification of the Dutch artist Escher’s *Circle Limit III* using the semi-regular $5 \cdot 3 \cdot 5 \cdot 3 \cdot 5 \cdot 3$ tiling exhibited in the Poincare model of hyperbolic geometry (Dunham, 1991). The use of *Mathematica* packages (Knezevic, et al, 2002; Sremcevic, et al, 2002) allows for numerous constructions and investigations of tilings on the Poincare’ model before the formulation of the proof on the symmetry group of the uncolored tiling (De las Penas, et al, 2006). The group of symmetries happens to be generated by the reflections with axes passing through the sides of a fundamental triangle and 5- and two 3- fold rotations with centers on vertices of a fundamental triangle.

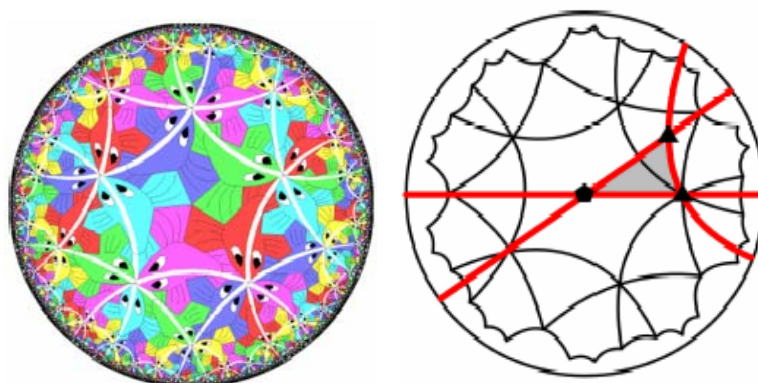


Figure 16: The $5 \cdot 3 \cdot 5 \cdot 3 \cdot 5 \cdot 3$ tiling superimposed on a modification of Escher’s *Circle Limit III*; finding symmetries of the $5 \cdot 3 \cdot 5 \cdot 3 \cdot 5 \cdot 3$ tiling on a fundamental triangle

8. Concluding Remarks

The study and formulation of proofs to mathematical problems is constantly a challenge to students in mathematics. As teachers, we strive to impart to our students the confidence from their

routine of problem solving and proving. This will make them interested to study mathematics and appreciate the meaning of proofs in existing and new mathematical theories. Technology plays a major role in providing a student learning support in the study and formulation of mathematical proofs. In this paper, our intent is to highlight some areas where students can be engaged in various levels of proving with technology, mostly results from our practices and experiences. While we draw attention to the use of technology in the study of proofs in this work, we realize that there is still a lot to be studied in terms of strategies of proving with technology and their usefulness on student learning.

References

- [1] ____, Count the trains, from www.mast.queensu.ca/~idis303/course-notes-m/trainproofs.pdf. Retrieved July 15, 2007.
- [2] Castellanos, J., Austin, J.D., & Darnell, E. (1994) *Non-Euclid*, from <http://cs.unm.edu/~joel/NonEuclid/NonEuclid.html>. Retrieved September 19, 2007.
- [3] De Las Peñas, M.L.P., G. R. Laigo, and E.B. Provido. (2006). *Studying Non-Euclidean Tilings and their Groups with the Aid of Technology* in the 11th Asian Technology Conference in Mathematics Proceedings (Sung Chi Chu, et al, Eds). USA: ATCM, Inc.
- [4] De Villiers, M. (2003) *Rethinking Proof with Geometers Sketchpad*. CA: Key Curriculum Press.
- [5] Dunham, Douglas (1991) *Transformations of Hyperbolic Escher Patterns* in Visual Mathematics, Vol 1 No 1, from <http://www.mi.sanu.ac.yu/vismath/dunham/index.html>. Retrieved July 15, 2007.
- [6] Foster, K. (1999, January 24). Re: Conjectures that are true for large n but are actually false. Message posted to <http://www.math.niu.edu/~rusin/known-math/99/smallnums>.
- [7] Hohenwarter, M. (2001) *Geogebra*, from <http://www.geogebra.org/cms/>. Retrieved December 20, 2006
- [8] Knezevic, I., R. Sazdonovic, and S. Yukminovic. (2002). *Basic Drawing in the Various Models of the Lobachevskian Plane for Mathematica 4.0*, from <http://library.wolfram.com/infocenter/MathSource/4260/>. Retrieved July 15, 2007.
- [9] Levasseur, K. and Hibbard, A. (1999) *Exploring Abstract Algebra with Mathematical*, Springer Verlag, NY.
- [10] Posamentier, A. (1999) *Teaching Secondary School Mathematics*, 5th ed. NJ: Prentice Hall.
- [11] ____, Primality Test, from http://www.bigprimes.net/primality_test.php. Retrieved July 15, 2007.
- [12] Reynolds, B. and Fenton, W. (2006) *College Geometry Using the Geometer's Sketchpad*. CA: Key Publishing.
- [13] Rivera, F.D. (2005). The Anthropological Account of the Emergence of Mathematical Proof and Related Processes in Technology-Based Environments. In Masalski, W. and Elliot, P. (Eds.) *Technology-Supported Mathematics Learning Environments*, 67th Yearbook of the National Council of Teachers of Mathematics (NCTM). VA: NCTM, Inc.
- [14] Sremcevic, M. and R. Sazdonovic. (2002). *Tesselations of the Euclidean, Elliptic and Hyperbolic Plane for Mathematica* from <http://library.wolfram.com/infocenter/MathSource/4540>. Retrieved July 15, 2007.

Two Explorations with Cabri 3D Leading to Two Theorems

Jean-Jacques Dahan

jjdahan@wanadoo.fr

IREM of Toulouse

France

Abstract: Exploring the volume of the convex envelope of a net of a cube with Cabri 3D, as the net opens and closes will lead to a conjecture about the maximum of this volume. We will prove this conjecture. We will also solve experimentally the problem of the tessellation of a cylinder with equilateral triangles after the observation of a picture taken in the convention Center of Hong Kong. The proof will be exposed. Eventually we will present quasi-tesselations to illustrate the Schwarz paradox in relation with the lateral area of a cylinder.

1. A problem of maximum of convex envelope

1.1. The problem generated with the Cabri 3D environment

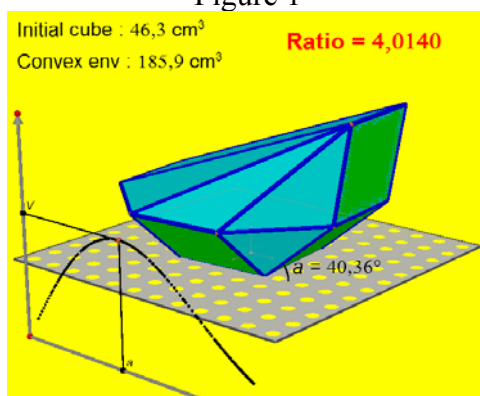
The net of a cube is created using Cabri 3D and the convex hull of this net is also created. The problem is: when is the volume of this convex hull the maximum?

1.2. The experimentations leading to a conjecture

The ratio between the volumes of the convex hull and the initial cube is computed and displayed (Figure 1). The angle a (units : degrees) between the horizontal plane and a lateral side is measured and displayed. As we can modify the angle a , we can find a position for the cube net which maximizes this ratio. The maximum volume ratio seems to be close to 4. The angle displayed by Cabri 3D for this maximum is $40,31^\circ$.

We have also linked the graph of function $V(a)$ to the convex hull to improve the understanding of the phenomenon.

Figure 1



1.3. The Cabri 3D power of construction to visualize the inside of a convex polyhedron

In order to validate the previous conjecture with a proof, we need to create an expression for the volume of the convex hull involving the angle a . This can be obtained by cutting the convex polyhedron into several parts of known volume, as shown in the Cabri 3D screenshots that follow

(Figures 2, 3 and 4) :

Figure 2

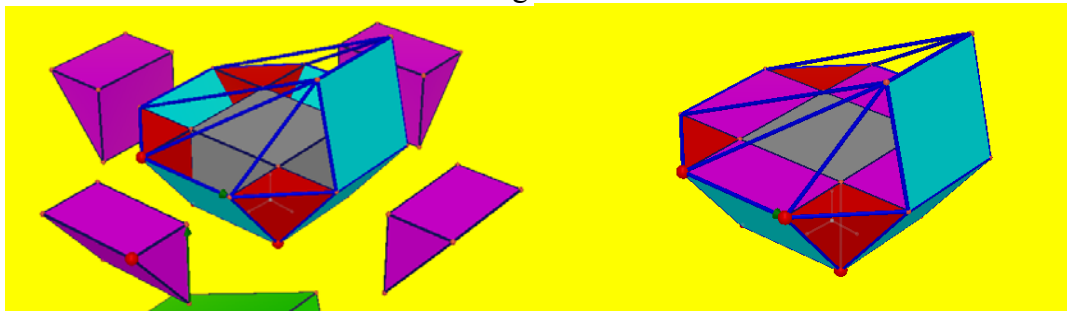


Figure 3

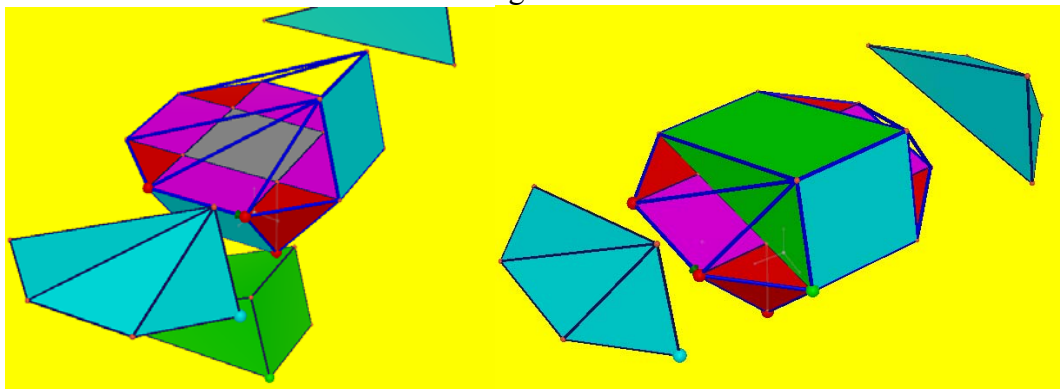
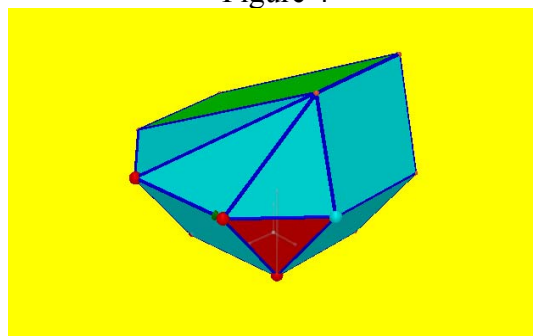


Figure 4



1.4. Symbolic proof validating the Cabri 3D conjecture

Computations have been done with a cube of side length 1. Volumes depend on the angle a between a lateral side of the cube net and the horizontal plane.

Volume V_1 of the green prism	$V_1 = \frac{1}{2}(1 + 2 \cos(a)) \sin(2a)$
Volume V_2 of the two blue pyramids	$V_2 = \frac{2}{3}(\cos(a) + \cos^2(a)) \sin(2a)$
Volume V_3 of the four purple prisms	$V_3 = \sin(2a)$

Volume V_4 of the four red pyramids	$V_4 = \frac{1}{3} \cos(a) \sin(2a)$
Volume V_5 of the grey prism	$V_5 = \sin(a)$

Total volume of the convex hull : $V(a) = \frac{1}{6}(3 + 2 \cos(a))^2 \sin(2a) + \sin(a)$

Using the Voyage 200, we can obtain an approximation of the value of a corresponding to the maximum of function V :

This value is approximatively $40,141113^\circ$

The value of the maximum volume is approximatively $4,014137$

If we calculate the derivative function $V'(a)$ we obtain:

$$V'(a) = \frac{1}{3}(3 + 2 \cos(a))^2 \cos(2a) - \frac{2}{3}(3 + 2 \cos(a)) \sin a \sin(2a) + \cos(a)$$

The Voyage 200 also gives this formula.

It is not easy to solve for the value a_m of a such as $V'(a_m) = 0$, however.

2. Quasi-tessellations of a cylinder

Note : « quasi-tessellation » in this context refers to the approximation of a surface by polygons all of whose vertices lie on the surface.

2.1. A real problem provided by the real world

As I was visiting the gorgeous Hong Kong Convention Center in December 2006, I was attracted by a wonderful cylindrical lampshade. This is the first picture I took when I was going down one of the escalators (Figure 5).

Figure 5



2.2. A conjecture of the real world validated with Cabri 3D

The next picture (Figure 6) was the one I took when a math problem occurred to me. The tourist was becoming a researcher

Figure 6

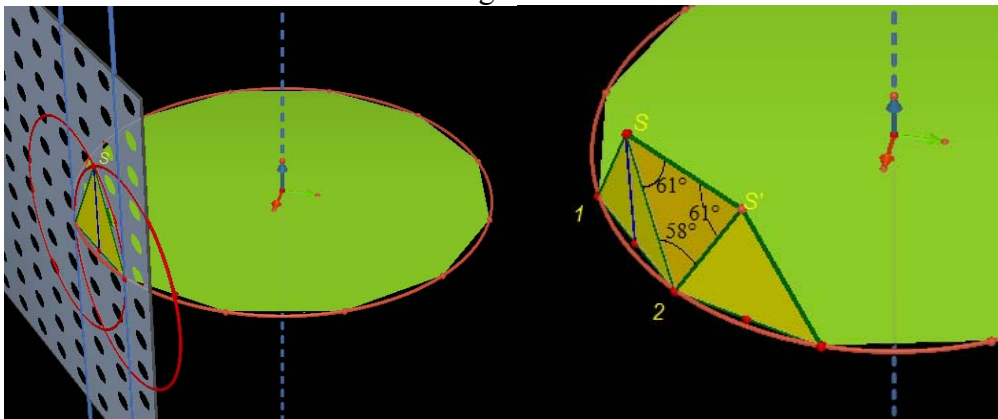


I noticed that the lampshade was based on a regular decagon on which the architect had placed vertical equilateral triangles. My question was:

Is this lampshade built with equilateral vertical triangles and where is the cylinder that I seem to see when I look at it?

So, back in my hotel I sat in front of my laptop to construct the first figure below. On one side of a regular decagon, I built a vertical equilateral triangle. To start the tessellation that I had conjectured, I rotated this triangle around the vertical axis of the decagon to obtain a second vertical equilateral triangle (the angle of the rotation is defined in order to move point 1 to point 2). But when I created the triangle linking these two triangles, I found that its angles measured $61^\circ, 61^\circ$ and 58° . So my conjecture was not validated.

Figure 7



I hence decided to try another experiment: instead of constructing a vertical equilateral triangle on one side of the regular decagon, I built one having its third vertex on the cylinder which is the product of the circle in which the decagon is inscribed and the vertical axis of the decagon. The second figure below shows that the conjecture seemed to be validated. So I decided to continue the construction to obtain a really good model of the lampshade in the Convention Center. This convinced me that my second conjecture was correct.

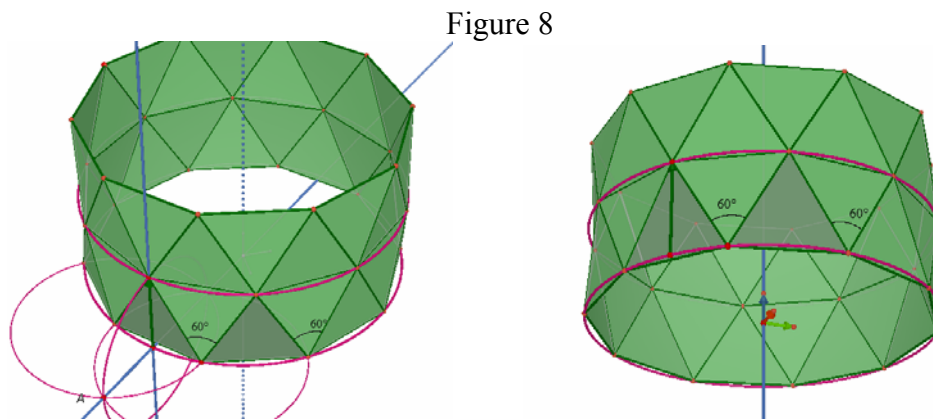


Figure 8

2.3. A generalisation of this conjecture with its Cabri-proof

A few months later, I received an email from a Belgian colleague telling me that his son (aged ten) had used a game called Magnetix to build a solid in the same way with only one difference: he started with an octagon instead of a decagon. This colleague was very proud of his son but asked me this question: is the construction done by his son mathematically correct?

I decided to use Cabri 3D to repeat my construction with other regular polygons and obtained the same validation. The diagram below shows the construction for a regular polygon with 20 edges. (Figure 9). That was a Cabri-proof, a validation using the mathematical background of the software. This property is still plausible at the level of nearly 100% in the meaning of Polya.

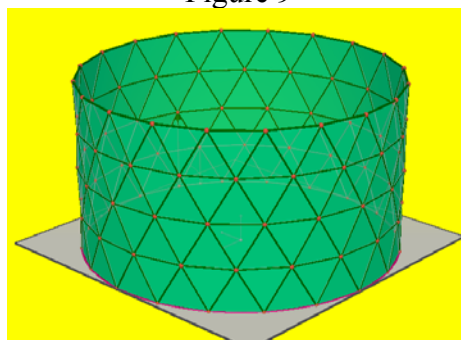


Figure 9

2.4. The quasi-tessellation of a cylinder with equilateral triangles (proof)

We have chosen to start with a polygon with n edges, so angle AOB is measured with $2\pi / n$

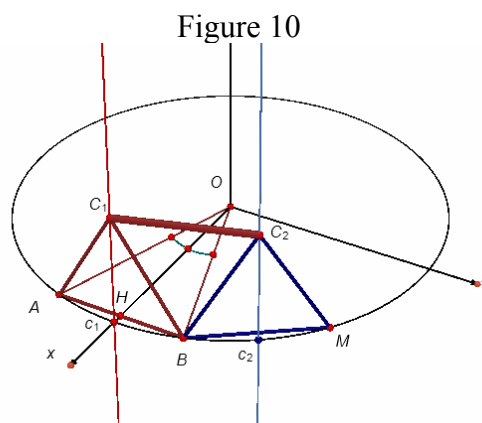


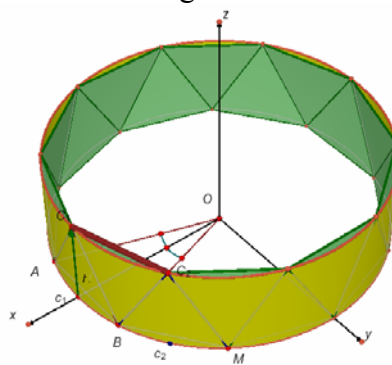
Figure 10

In this figure we can see that segment c_1c_2 is the image of the segment $[AB]$ upon a rotation about the z axis by angle $\frac{\pi}{n}$. Hence $c_1c_2 = AB$, So the quadrilateral $C_1C_2c_2c_1$ is a rectangle and $c_1c_2 = C_1C_2$. The point C_1 can be chosen anywhere on the perpendicular through c_1 and in the construction shown has been chosen so that $AB = AC_1 = BC_1$. Similarly, $AB = BM = BC_2$ and hence the triangle BC_1C_2 is equilateral. That is the end of the proof.

2.5. The impossibility of approximating a cylinder by a quasi-tessellation with isosceles triangles (Schwarz paradox)

The area of one of these triangles is $r^2\sqrt{3}\sin^2\frac{\pi}{n}$. All around the circle we can put $2n$ triangles (figure below: n like ABC_1 and n like BC_1C_2) having $A_t(n) = 2nr^2\sqrt{3}\sin^2\frac{\pi}{n}$ as an area. These triangles are attached to a cylinder having the visible circle as a basis and C_1c_1 as height.

Figure 11



This height is the number h obtained with the coordinates in the system of axis (Ox, Oy, Oz) :

As we have, $C_1 \begin{bmatrix} r \\ 0 \\ h \end{bmatrix}$ and $B \begin{bmatrix} r \cos(\frac{\pi}{n}) \\ r \sin(\frac{\pi}{n}) \\ 0 \end{bmatrix}$, h is given by the equation :

$C_1B = AB = 2r \sin(\frac{\pi}{n})$ or :

$(r - r \cos(\frac{\pi}{n}))^2 + (r \sin(\frac{\pi}{n}))^2 + h^2 = 4r^2 \sin^2(\frac{\pi}{n})$. The solution is:

$$h = r\sqrt{2} \sin(\frac{\pi}{n})$$

Let us evaluate the lateral area of this cylinder:

$A_c(n) = 2\pi r \cdot r\sqrt{2} \sin(\frac{\pi}{n}) = 2\pi r^2\sqrt{2} \sin(\frac{\pi}{n})$

To check mathematically if these triangles can approach the cylinder as n grows larger, we can evaluate the limit of the ratio $\frac{A_t(n)}{A_c(n)}$ as n goes to infinity.

As $\frac{A_t(n)}{A_c(n)} = \frac{n\sqrt{3} \sin(\frac{\pi}{n})}{\pi\sqrt{2}}$, this limit is $\frac{\sqrt{3}}{\sqrt{2}}$ which is close to 1.2 (1.224744871).

The conclusion is that it is impossible to tile a cylinder in such a way with equilateral triangles, even in the limit as n goes to infinity.

A generalization of this problem is to explore whether it is possible with isosceles rather than equilateral triangles. To solve it we can put c_1 on the same vertical but at a height $h_\alpha = \alpha h$.

The new $A_t(n)$ is $2\pi r h_\alpha = 2\pi r \alpha h = 2\pi r^2 \sqrt{2} \alpha \sin(\frac{\pi}{n})$.

The new length of c_1H is given by $\sqrt{r^2 \sin^2(\frac{\pi}{n}) + h^2 \alpha^2}$ and hence :

$$2nr \sin(\frac{\pi}{n}) \sqrt{r^2 \sin^2(\frac{\pi}{n}) + h^2 \alpha^2} = 2nr \sin(\frac{\pi}{n}) \sqrt{r^2 \sin^2(\frac{\pi}{n}) + 2r^2 \alpha^2 \sin^2(\frac{\pi}{n})}$$
 and at last

$$A_t(n) = 2nr^2 \sin^2(\frac{\pi}{n}) \sqrt{1 + 2\alpha^2}$$

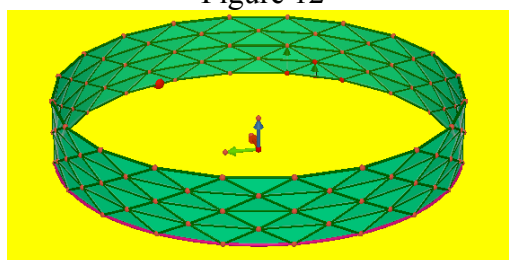
So $\frac{A_t(n)}{A_c(n)} = \frac{2nr^2 \sin^2(\frac{\pi}{n}) \sqrt{1 + 2\alpha^2}}{2\pi r^2 \sqrt{2} \alpha \sin(\frac{\pi}{n})}$ an its limit as n goes to infinity is $\frac{A_t(n)}{A_c(n)} = \frac{\sqrt{1 + 2\alpha^2}}{\sqrt{2}\alpha}$.

As this limit is always strictly more than one, it is impossible to approach the area of a cylinder with the area of a tessellation with such isosceles triangles.

Remark: the curve of the function $x \rightarrow \frac{\sqrt{1 + 2x^2}}{\sqrt{2}x}$ shows that when α is close to 0 the previous ratio

has a very large value indicating that the area of our quasi-tessellation is very big in comparison to the area of the cylinder. This result is an illustration of the Schwarz paradox which shows that limits of surfaces do not have the same properties as limits of lengths: the perimeter of the regular polygon inscribed in the base circle of the cylinder will approach the circumference of this circle as the number of sides goes to infinity, but the area of the related quasi-tessellation of isosceles triangles will not converge to the area of the cylinder as the number of sides goes to infinity. However, as the limit of this function when x goes to infinity is 1, the area of the quasi-tessellation approaches the area of the cylinder for large values of α (i.e. for triangles with a small base and a huge altitude).

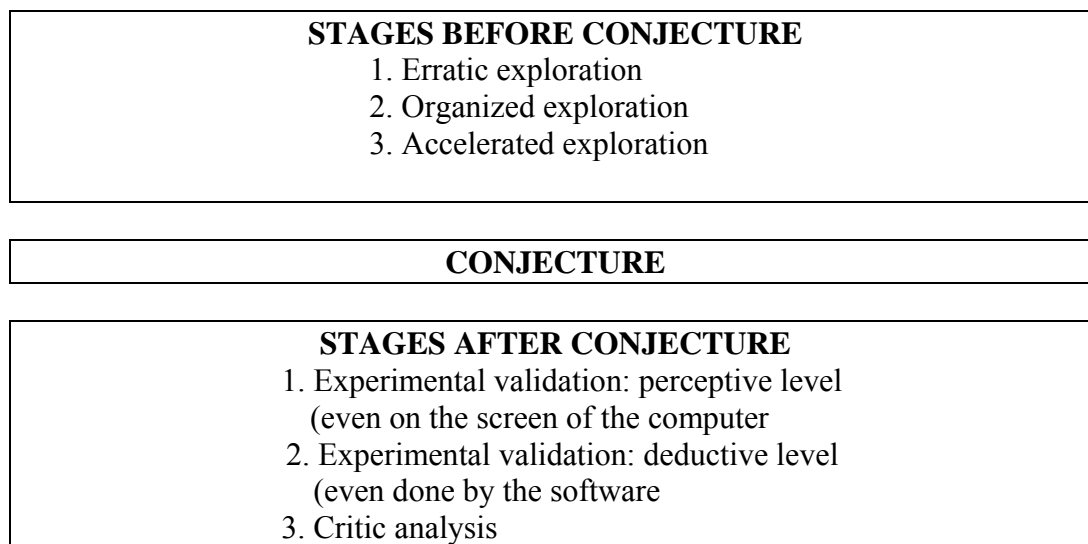
Figure 12



3. A theoretical presentation of these two explorations

3.1. The experimental process of discovery (Dahan's model)

According to the results of Dahan's work (thesis of Ph D) a model of the different stages of the work of a researcher during the experimental process of discovery of a math problem is given by :



3.2. Techniques of validation and levels of geometry during such a process (Parszyz and Dahan's praxeologies)

3.2.1. Chevallard's praxeologic organizations

According to Chevallard, one way to understand the building of knowledge(s) is the notion of praxeology which consists of four things: a task (a problem to solve), a technique (one way to perform this task), a technology (one mathematical justification of the technique, very often a theorem) and a theory ((which is the overall discourse generating the previous justification).

3.2.2. Parzysz' praxeologies G1 and G2

In the particular case of geometric problem solving in paper and pencil environment, Parzysz has shown two particular praxeologies:

G1 or "Level of geometry 1" where the technique is essentially perceptive and the technology a justification based principally on visual superimposition. The theory could be based on the accuracy of the technical tools used (rule, compass, protractor).

G2 or "Level of Geometry 2" where the technique is demonstrative proof and the technology is the theorems on which the proof is based.

3.2.3. Dahan's praxeologies

Dahan has extended the Parzysz praxeologies G1 and G2 into G1 and G2 Informatique because G1 and G2 are not sufficiently detailed to describe what happens when working on a screen with a geometric software.

G1 Informatique : The level G1 Informatique is based on perceptive validations on the screen of the computer. There is a huge difference between paper and pencil exploration and researching by means of a computer with DGS: what we can perceive on the screen of the computer has nothing to see with what we can perceive during an exploration with paper an pencil (recognizing that points are collinear, recognizing that a locus is a parabola , a circle...). Accuracy is better and a window is opened to conjectures that cannot be obtained using paper and pencil.

G2 Informatique : At the level G2 Informatique, proof is based on the properties given by the software. When using a DGS like Cabri, it is possible to validate conjectures with tools of very high

level of accuracy : it is possible for the software to recognize that points are collinear, that lines are perpendicular, to recognize circles, conics, to give the equations of lines, circles, planes, spheres. This is a deductive level because everything that the software returns to the user is the mathematical consequences of the hypotheses given during the constructions. So, there is a level where DGS and the user are a couple generating the results that a normal deductive reasoning can give. is not exactly the symbolic proof built by the human being.

Dahan, in his work about the experimental process of discovery (thesis of Ph. D.) has checked that the previous model describing the stages of such a process DGS, can help us to understand what the researcher is doing when exploring and at what level of validation.

3.3. A didactical description of the two previous explorations

3.3.1. First problem

The exploration starts immediately with accelerated exploration because the tools of Cabri 3D enable constructions, measurements and manipulations that are impossible with paper and pencil. The level is G1 Informatique because the conjecture arises out of perception and is validated perceptively by checking on the screen the variations of the volume of the envelope of the open cube.

The construction of the curve of the function giving the volume is at level G1 informatique because, the curve displayed on the screen gives us a perceptive validation of the conjecture done. No validation at the level G2 Informatique.

Deriving the formula for the volume of the convex envelope was an activity at G2 level (deductive validation with paper and pencil). However, this formula was difficult or impossible to solve analytically and hence the researcher came back to level G2 informatique and used the Voyage 200 to validate the conjecture that the maximum was reached for a number close to 4.

So, this example was an example where the researcher after an experimental validation in G1 Informatique with a DGS was led to the symbolic proof in G2. But, as this proof was impossible to be done analytically, he came back to G2 Informatique with a CAS.

3.3.1. Second problem

As this exploration started with an idea that was tested using the software, it starts with organized exploration at level G2 Informatique. Validation is done using the Cabri tool “angle measurement” to test if a particular angle is 60° . This angle is not 60° , and hence the conjecture, invalidated, is rejected. The accelerated exploration is led when the researcher has the impression to approach the solution of the problem and when he tries very quickly to validate necessary conditions deduced from the conjecture. Usually the validations are perceptive, so in G1 Informatique but here it is still a validation in G2 Informatique.

We cannot observe the stages after conjecture because these stages are a bit included in the previous one. Another reason is because the researcher is an expert and the problem to solve is not an open ended problem.

The proof given by symbolic calculation with coordinates is at level G2.

3.4. Conclusion

One of the problem not solved by Dahan’s thesis is: how can we teach with DGS for example, in order to convince students not to stop their work by validating a conjecture in G2 Informatique but to come back to G2 to give the usual symbolic and deductive proof? The two explorations we have described can give a beginning of solution for this problem. Probably, we must choose exploration situations where the students will feel doubtful about the validations the software can allow them to do.

References

- [1] POLYA G., 1967, *La découverte des Mathématiques*, Dunod, Paris.
- [2] LAKATOS I., 1984, *Preuves et réfutations Essai sur la logique de la découverte en mathématiques*, Hermann, Paris.
- [3] JOSHUA M.A., JOHSUA S., 1987, Les fonctions didactiques de l'expérimental dans l'enseignement scientifique (première partie) in *Recherches en didactique des mathématiques*, 8, (3), 231-266, La Pensée Sauvage éditions.
- [4] JOSHUA M.A., JOHSUA S., 1987, Les fonctions didactiques de l'expérimental dans l'enseignement scientifique (deuxième partie) in *Recherches en didactique des mathématiques*, 9, (1), 5-30, La Pensée Sauvage éditions.
- [5] POLYA G., 1989, *Comment poser et résoudre un problème*, Éditions Jacques Gabay, Paris.
- [6] MILLAR R., 1996, Investigations des élèves en science : une approche fondée sur la connaissance in *Didaskalia* N° 9, 9-30
- [7] CHEVALLARD Y., 1998, La notion d'organisation praxéologique, in Actes de l'Université d'été de La Rochelle, *Analyse des pratiques enseignantes et didactique des mathématiques*, IREM de Clermont-Ferrand.
- [8] TROUCHE L., 1998, *Expérimenter et prouver Faire des Mathématiques au lycée avec des calculatrices symboliques ?*, IREM de Montpellier.
- [9] HOUEMENT C., KUZNIAK A., 1998-99, Géométrie et paradigmes géométriques, Petit X N° 51, IREM de Grenoble.
- [10] PARZYSZ B., 2001, Articulation entre perception et déduction dans une démarche géométrique en PE1, in *Colloque de la COPIRELEM, Tours 2001*, Presses de l'université d'Orléans, IREM d'Orléans.
- [11] DAHAN J.J., 2001, Chapitre 13 : Un exemple de transposition de problème inversé en classe, in *Enseigner et pratiquer les Mathématiques avec Cabri : tome 1*, Brochure de l'IREM de Toulouse 165.
- [12] DAHAN J.J., 2002, 3 exemples pour illustrer la démarche expérimentale en mathématiques avec Cabri, in *Enseigner la géométrie dans le secondaire, Actes du colloque Inter-Irem Géométrie*, Liège, 133-158.
- [13] OLIVERO F., 2002, The proving process within a dynamic geometry environment, thesis of Ph. D., Bristol University, UK.
- [14] PARZYSZ B., 2003, Articulation et déduction dans une démarche géométrique en PE1, in *Concertum. Dix ans de formation des professeurs des écoles en mathématiques*. Tome 2 (Démarches et savoirs à enseigner) chap. 1 (Espace et géométrie), 107-125. Ed. ARPEME.
- [15] DAHAN J.J., 2005, La démarche de découverte expérimentalement médiée par Cabri-géomètre en mathématiques. Un essai de formalisation à partir de l'analyse de démarches de résolutions de problèmes de boîtes noires, thesis of Ph. D., *Joseph Fourier University*, Grenoble, France. <http://www-iam.imag.fr/ThesesIAM/ThesejjDahan.pdf>
- [16] DAHAN J.J., 2007, Examples showing the new possibilities of the new version of Cabri 3D for all levels, in *the proceedings of the T3 Congress of Chicago (CD)*. <http://www.baskow.com/client/t32007/handouts/Saturday/409-DAHAN.pdf>

Application of Network Simplex Method to Currency Arbitrage Detection

Amanda Soon Wanmei

wmsoon@nie.edu.sg

Mathematics and Mathematics Education
National Institute of Education
Nanyang Technological University
Singapore

Abstract: In this paper, we use a binary integer programming model to detect currency arbitrages. This problem has a special structure, which allows us to apply the network simplex algorithm. Using Matlab, a program modelled on this algorithm was constructed to detect currency arbitrages involving numerous pairs of exchange rates.

1. Introduction

Previously in [4], a Binary Integer Programming (BIP) model was introduced to detect currency arbitrages. In this work, we present a modified BIP model and use a customized Matlab program to detect currency arbitrages involving online exchange rates. (The reader can refer to [1] and [6] for references on Matlab.) This program is modelled on the efficient network simplex method.

A currency exchange rate is the relative value between two currencies. Typically, such rates are expressed in terms of “bid” and “ask” (or “sell” and “buy”) prices. The bid price is the amount that a seller obtains in the quote currency (e.g., US dollar), when he sells one unit of the base currency (e.g., Euro). On the other hand, the ask price is the amount that a buyer needs to pay in the quote currency, to obtain one unit of the base currency.

For clarity of explanation, a typical example of a table of exchange rates found on the internet is given in the figure below. From the figure, we see that for the currency pair EUR/USD, the bid and ask prices are 1.3827 and 1.3829 respectively. Thus we can sell 1 euro to obtain 1.3827 US dollars, or buy 1 euro with 1.3829 US dollars.



Currency Pair	Bid	Ask
EURUSD	1.3827	1.3829
USDCHF	1.2007	1.2010
USDJPY	121.25	121.27
GBPUSD	2.0561	2.0564
AUDUSD	0.8801	0.8804
USDCAD	1.0485	1.0489

Figure 1.1 A snapshot of some online exchange rates.

As the ask prices are usually slightly higher than the bid prices, losses are usually incurred when we convert money from a base currency to a quote currency and then back. Nevertheless, making use of possible differences in the exchange rates among different financial markets, a chain of currency conversions may result in a gain in the base currency. Such an opportunity is called a *currency arbitrage*. For example, if r_{ij} is defined as the exchange rate for converting currency i to currency j , and if $r_{ij}r_{jk} \cdots r_{pq}r_{qi} > 1$ (for some $q \neq p \neq \dots \neq k \neq j \neq i$), then, by definition, the currency conversion sequence $i \rightarrow j \rightarrow k \rightarrow \dots \rightarrow p \rightarrow q \rightarrow i$ constitutes a currency arbitrage.

Currencies are traded on the foreign exchange market, and are affected by the supplies and demands for them. The supply and demand for currencies arise from the needs of import or export companies, foreign investors, speculators and central bankers. An increase in the supply of (or demand for) a currency will make it less valuable (or more valuable) relative to other currencies, leading to changes in the exchange rates. For example, suppose an export company in Canada sells its products to a large Japanese firm. As the contract will probably be negotiated in Japanese yen, the Canadian company will receive its revenue in a currency that is of limited use outside of Japan. Hence it needs to sell its yen to exchange for Canadian dollars (to pay labour costs, etc). The supply of yen on the foreign exchange market will then increase, while the supply of Canadian dollars decreases. This causes the Canadian dollars to appreciate in value and the yen to depreciate. So for example, the JPY-USD exchange rate will decrease while the CAD-USD rate increases. Though most of the time all the exchange rates will be synchronized so that arbitrage cycles do not occur, occasionally this will not be so, allowing arbitrageurs to make a profit.

The problem of identifying currency arbitrage opportunities has been studied previously. A widely known mathematical model used for this purpose is the generalized circulation problem (GCP). This problem is a generalization of the maximum flow problem in which a source node is specified, and the amounts of flow entering and leaving an arc are linearly related (see e.g., [2]). In addition, every node, except for the source node, has to satisfy a flow balance constraint. When applied to the detection of currency arbitrages, the nodes correspond to the different currencies, the arcs correspond to the different currency conversions and the gain factor represents the currency exchange rate. The objective is then to find the combination of flows or conversions that maximizes the excess for a currency arbitrage problem at the source node. This formulation is simple, but we believe that an improvement is possible.

A binary integer programming model to detect currency arbitrages was first introduced in [4]. In that paper, it was assumed that all pairwise currency exchange rates were known. In practice, it happens that certain pairs of currencies are not accessible for trade by a given trader. In this paper, a modified binary integer programming (BIP) model is introduced to deal with such a situation. This BIP model can be reduced to a simple linear program (LP). The network simplex method can be employed to solve this LP by exploiting its special structure. Since solving this LP is equivalent to solving the original BIP model, in essence, we are using the network simplex algorithm to identify currency arbitrages. The simplicity and efficiency of the network simplex method is commonly known; it compares favorably with the methods that can be used to solve the GCP (e.g., the conventional simplex method). In addition, using this method allows us to conduct sensitivity analysis and to easily detect arbitrages (if they exist) when the exchange rates change - which happens in real-time situations.

This paper is organized as follows. We first present the generalized circulation problem formulation and mention some issues inherent in the model. Following that, we discuss our BIP model and describe the network simplex method used for currency arbitrage detection. The

application of our model to a numerical example will then be discussed using online exchange rates.

2. A Generalized Circulation Problem (GCP) formulation

Suppose that there are m currencies considered. We denote r_{ij} as the given exchange rate between currencies i and j , for $i, j = 1, \dots, m, j \neq i$. That is, r_{ij} represents the amount of currency j that can be exchanged for one unit of currency i . For example, from the snapshot in Figure 1.1, supposing that currencies 1 and 2 denote EUR and USD respectively, then $r_{12} = 1.3827$ and $r_{21} = 1/1.3829$.

In this problem, the decision variables u_{ij} are defined to be the amount of currency i to convert to currency j , for $i, j = 1, \dots, m, j \neq i$.

The currency arbitrage detection problem has been formulated as a GCP in the past. (cf. [3] (chapter 9) and [5] (page 255)). It is actually a generalization of the maximum flow problem, in the sense that a unit of flow leaving one node arrives at the next node multiplied by a scale factor. In our application, each node represents one currency. The flow leaving node i for node j is u_{ij} , the scale factor is the currency conversion rate r_{ij} , and the flow arriving at node j from node i is $r_{ij}u_{ij}$.

The main idea behind this problem formulation is the following. We choose a base currency and represent it by a node called the base node. A supply of one unit from the base node (without loss of generality, let it be node 1) is assumed. If the inflow to the base node is finite and larger than one unit, i.e., there is a net inflow, then an arbitrage involving the base currency has been found. Thus the aim is to maximize the flow excess at the base node, after the single unit circulates within the currency exchange network. Note that at all the nodes (except for the base node), the flows must be conserved.

We summarize the above in the following GCP formulation:

$$\begin{aligned} \max \quad & f = \sum_{i=2}^m r_{i1}u_{i1} - 1 \\ \text{s.t} \quad & \sum_{i=2}^m u_{1j} = 1, \\ & \sum_{j \neq k} u_{kj} - \sum_{i \neq k} r_{ik}u_{ik} = 0 \quad \text{for } k = 2, \dots, m, \\ & u_{ij} \geq 0 \quad \text{for } i, j = 1, \dots, m, j \neq i. \end{aligned}$$

However, there are some inherent difficulties in this GCP formulation. For example, the problem will be unbounded if currency arbitrages involving currencies other than the base currency occur. (See [4] for details.) In addition, a new issue we notice is that, in using the GCP above, the information on all pairwise currency exchange rates is required.

3. A modified Binary Integer Programming model and its relaxed version

The aim of our proposed BIP model is to provide a more efficient method to detect possible currency arbitrages, while, at the same time, avoiding the issues surrounding the GCP formulation as mentioned earlier. Let r_{ij} be the given currency exchange rates defined as before.

We modify the BIP model in [4] to incorporate the situations where not all pairwise currency exchanges are feasible. Suppose that A is the set of all (i, j) ($i, j = 1, \dots, m, j \neq i$) such that the rate r_{ij} is usable.

Denote the decision variables

$$x_{ij} = \begin{cases} 1, & \text{if currency } i \text{ is converted to currency } j; \\ 0, & \text{otherwise,} \end{cases}$$

for $(i, j) \in A$.

The modified model is then

$$\begin{aligned} \max \quad & z = \sum_{(i,j) \in A} (\log r_{ij}) x_{ij} \\ \text{s.t} \quad & \sum_{\{j:(i,j) \in A\}} -x_{ij} + x_{ji} = 0, \quad \text{for } i = 1, \dots, m, \end{aligned} \tag{3.1}$$

$$x_{ij} = 0 \text{ or } 1, \quad \text{for } (i, j) \in A. \tag{3.2}$$

The constraints present in (3.1) are the flow conservation constraints. That is, at each (currency) node i , $i = 1, \dots, m$, the inflow must be equal to the outflow. These constraints are necessary since each set of currency exchanges forms a loop (cycle). It can be shown that a currency arbitrage exists if and only if the optimal objective value of this problem is positive. This is essentially due to the fact that the objective function above can be rewritten as $\log \prod_{(i,j) \in A} r_{ij}^{x_{ij}}$, and so maximizing

$\sum_{(i,j) \in A} (\log r_{ij}) x_{ij}$ is the same as maximizing $\prod_{(i,j) \in A} r_{ij}^{x_{ij}}$. Hence $\exists q \neq p \neq \dots \neq k \neq j \neq i$ such that $r_{ij} r_{jk} \cdots r_{pq} r_{qi} > 1$, if and only if $x_{ij} = x_{jk} = \dots = x_{pq} = x_{qi} = 1$ and $\log r_{ij} + \log r_{jk} + \dots + \log r_{pq} + \log r_{qi} > 0$. Note that this problem always has a feasible solution ($x_{ij} = 0, \forall (i, j) \in A$). In addition, it always has a bounded optimal objective value. For more details, see [4].

Now we can easily relax the integer constraints present in (3.2) to the linear constraints

$$0 \leq x_{ij} \leq 1, \quad \text{for } (i, j) \in A, \tag{3.3}$$

to form the relaxed problem BIP-R, due to the following property.

Primal integer solution property: Since the right hand side of the constraints in (3.1) and the upper bounds on the variables in (3.3) are all integers, all basic feasible solutions to the BIP-R

model are integer-valued (see [5]). That is, x_{ij} takes the value of either 0 or 1. This implies that solving the relaxed linear programming problem is *equivalent* to solving the original integer programming problem.

4. Application of the network simplex method to solve BIP-R

The BIP-R can be viewed as a network flow problem which corresponds to a graph with m nodes and directed arcs connecting them. Due to the problem's special simple structure, we can employ the network simplex method. We discuss the method (specific to our problem) below. For convenience, we use c_{ij} to denote the coefficients in the objective function of the BIP-R, i.e., $c_{ij} = \log r_{ij}$ for all $(i, j) \in A$.

Before we start the network simplex method, we need an initial basic feasible solution. It can be observed that as USD is the dominant currency in international markets, the exchange rate between USD and any other currency will be accessible. Thus we can let USD be currency 1 (arbitrarily) and choose the starting basic variables to be x_{1j} , for $j = 2, \dots, m$. [Note however, in the event that currency trading is done in some restricted market which does not involve a dominant currency, we can still find an initial basic feasible solution easily. One way is to use an idea similar to the Big-M method. That is, we can create an artificial node $(m+1)$ which connects to all currency nodes through directed artificial arcs, and then set the starting basic variables to be $x_{m+1,j}$, for $j = 1, \dots, m$. The corresponding objective coefficients are set to be $c_{m+1,j} = -M$, for $j = 1, \dots, m$ (where M is a very large number), and the constraints $\sum_j -x_{m+1,j} = 0$, $x_{m+1,j} \geq 0$, for $j = 1, \dots, m$ are added. The network simplex method can then be applied to this modified problem.]

Initialization. Let $t = 0$. We set $x_{ij}^0 = 0$ for all $(i, j) \in A$. Let B^t denote the set of all the ordered pairs (i, j) corresponding to the basic x_{ij}^t variables, i.e., $B^t = \{(i, j) \in A \mid x_{ij}^t \text{ is basic}\}$. We set $B^0 = \{(1, j) \mid j = 2, \dots, m\}$.

1. Calculations of dual variables and reduced costs.

We solve the equations $-y_i^t + y_j^t = c_{ij}$ corresponding to all $(i, j) \in B^t$, where y_i^t is the dual variable for (the constraint corresponding to) the currency i . With $m-1$ equations and m unknown dual variables, we arbitrarily set one y_i^t to zero and solve for the other variables. Then we calculate the reduced costs of all $(i, j) \notin B^t$ via the equations $\bar{c}_{ij}^t = c_{ij} - (y_j^t - y_i^t)$.

2. *Termination rule.* If the reduced costs are non-positive (resp. nonnegative) for non-basic variables at their lower (resp. upper) bounds, the current basic feasible solution is optimal. That is, let $L^t := \{(i, j) \mid (i, j) \notin B^t, x_{ij}^t = 0 \wedge \bar{c}_{ij}^t > 0\}$ and $U^t := \{(i, j) \mid (i, j) \notin B^t, x_{ij}^t = 1 \wedge \bar{c}_{ij}^t < 0\}$. If $L^t = U^t = \emptyset$, we terminate the algorithm. Otherwise, go to Step 3.

3. *Choice of entering variable and determination of maximum change of flow.*

Use *Bland's rule* (see e.g. [5]) to choose the entering variable (arc):

Among all $(i, j) \in L^t \cup U^t$, choose the variable x_{ij} with the smallest i to enter. If there exists a tie, we choose the variable with the smallest j .

Let \bar{x}_{pq}^t be the entering variable. Then a cycle consisting of some current basic arcs and $\text{arc}(p, q)$ is formed. Find $S^t := \{(i, j) \in B^t \mid \text{arc}(i, j) \text{ is in the same direction as } \text{arc}(p, q) \text{ in the cycle}\}$, and $O^t := \{(i, j) \in B^t \mid \text{arc}(i, j) \text{ is in the opposite direction to } \text{arc}(p, q) \text{ in the cycle}\}$.

If $\bar{x}_{pq}^t = 0$, find $k^t = \max_{k \geq 0} \{k \mid x_{ij}^t + k \leq 1 \ \forall (i, j) \in S^t \text{ and } x_{ij}^t - k \geq 0 \ \forall (i, j) \in O^t\}$.

If $\bar{x}_{pq}^t = 1$, find $k^t = \min_{k \leq 0} \{k \mid x_{ij}^t + k \geq 0 \ \forall (i, j) \in S^t \text{ and } x_{ij}^t - k \leq 1 \ \forall (i, j) \in O^t\}$.

That is, we find the maximum possible change of flow k^t such that after increasing (or decreasing) the flows on the basic arcs in the cycle by k^t , the new flows will still be within the given bounds. Note that since all the variables in the basic feasible solution are equal to 0 or 1, the amount of change (k^t) must also be 0 or 1. Then we go to Step 4.

4. Updating of all flows and determination of leaving arc.

To update the flows, $\forall (i, j) \in S^t \cup \{(p, q)\}$, we set $x_{ij}^{t+1} = x_{ij}^t + k^t$. $\forall (i, j) \in O^t$, we set $x_{ij}^{t+1} = x_{ij}^t - k^t$. For all other arcs (i, j) , we set $x_{ij}^{t+1} = x_{ij}^t$. Then we identify all the arcs that block the change of flow in the cycle and choose the leaving arc among them.

That is, if $\bar{x}_{pq}^t = 0$, use Bland's rule to choose the leaving arc among the set $\{(i, j) \in S^t \mid x_{ij}^t + k^t = 1\} \cup \{(i, j) \in O^t \mid x_{ij}^t - k^t = 0\}$. If $\bar{x}_{pq}^t = 1$, use Bland's rule to choose the leaving arc among the set $\{(i, j) \in S^t \mid x_{ij}^t + k^t = 0\} \cup \{(i, j) \in O^t \mid x_{ij}^t - k^t = 1\}$. Suppose that the leaving arc is (r, s) . Set $B^{t+1} = (B^t \cup \{(p, q)\}) \setminus \{(r, s)\}$. We then have a new basic feasible solution and an updated set of basic arcs. Reset $t = t + 1$ and return to Step 1.

As exchange rates change all the time, it is desirable to be able to update the optimal solution to BIP (or rather BIP-R) easily in practice. Sensitivity analysis provides a good tool for this purpose.

Suppose that the new exchange rate of converting currency k to l is $r_{kl}' = \beta r_{kl}$, where r_{kl} is the original exchange rate. The new coefficient of x_{kl} in the objective function is then $c_{kl}' = \log(\beta r_{kl}) = c_{kl} + \log \beta$. (Note: for convenience, we append a prime to the parameters and variables of which the value will change due to the change of r_{kl} to r_{kl}' .) There are two possible cases in updating the reduced costs to find the new optimal solution. We will state them briefly here. For more details, see [4].

Case 1. x_{kl} is non-basic in the original optimal solution. Only the reduced cost of x_{kl} changes. That is, $\bar{c}_{kl}' = \bar{c}_{kl} + \log \beta$. We then check if \bar{c}_{kl}' satisfies the optimality conditions in Step 2 of the network simplex method. If yes, the current solution remains optimal. Otherwise, we re-optimize through further iterations of the network simplex algorithm.

Case 2. x_{kl} is basic in the original optimal solution. As some dual variables will change, the reduced costs of some variables change correspondingly. Let T_k be the subtree that contains

node k and T_l be the subtree that contains node l , after the arc (k,l) from the spanning tree corresponding to the original optimal solution is removed. The reduced cost \bar{c}_{ij} will not change if both nodes i and j fall within the same subtree (either T_k or T_l). Otherwise, if $i \in T_k$ and $j \in T_l$,

$$\bar{c}'_{ij} = \bar{c}_{ij} - \log \beta;$$

and if $i \in T_l$ and $j \in T_k$,

$$\bar{c}'_{ij} = \bar{c}_{ij} + \log \beta.$$

Once we update the reduced costs as above, we can continue with Step 2 of the network simplex algorithm to check for optimality, and to re-optimize if necessary.

Hitherto, we have discussed the BIP-R model formulation, the network simplex algorithm as applied to this model, and described the sensitivity analysis procedure. Now we will present a numerical example to clarify our explanations.

5. A numerical example using an online forex trading station

In this section, we apply a customized Matlab program modelled on the network simplex method, to solve our BIP-R problem in currency arbitrage detection. The data used were taken from an online forex trading system.

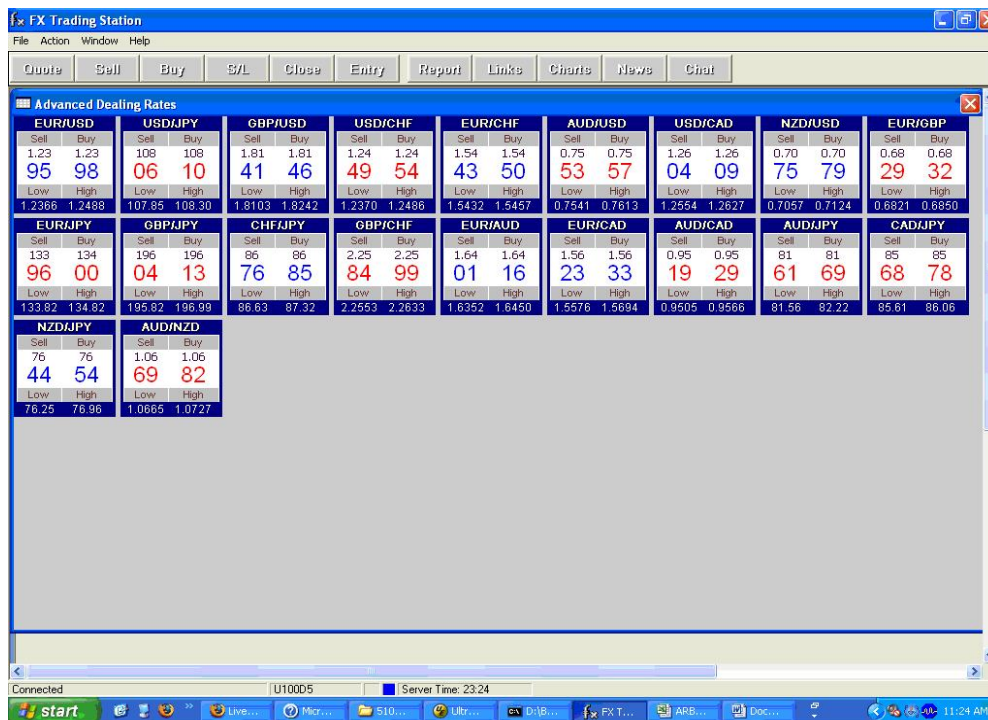


Figure 5.1 A snapshot of an online forex trading station

From the sell and buy (or bid and ask) prices given in Figure 5.1, we can obtain the table of exchange rates in Table 5.2. (Note that a dash indicates an unavailable rate.)

Let currencies 1, 2, 3, ... denote USD, EUR, JPY, ..., respectively. With the input of exchange rates from Table 5.2. into our Matlab program, the output optimal solution to the BIP-R model was $x_{25} = x_{42} = x_{54} = 1$ and $x_{ij} = 0$ for all other $(i, j) \in A$. (Recall that A is the set of ordered pairs (i, j) such that r_{ij} is available. E.g., $(1,2) \in A$ but $(2,8) \notin A$.) This corresponds to an arbitrage EUR \rightarrow CHF (Swiss francs) \rightarrow GBP (Great Britain Pounds) \rightarrow EUR with $r_{25}r_{54}r_{42} = 1.00022$. That is, changing each euro through this cycle leads to a gain of 0.00022 euro.

Note that corresponding to this solution, the set of optimal basic variables $B^* = \{x_{13}, x_{14}, x_{16}, x_{17}, x_{18}, x_{42}, x_{54}\}$, and the optimal reduced costs \bar{c}_{ij}^* (for $(i, j) \in A$) were also determined by the program.

Table 5.2 Exchange rates from a forex trading station

	USD	EUR	JPY	GBP	CHF	AUD	CAD	NZD
USD	1	0.8066	108.0600	0.5511	1.2449	1.3233	1.2604	1.4126
EUR	1.2395	1	133.9600	0.6829	1.5443	1.6401	1.5623	-
JPY	0.0093	0.0075	1	0.0051	0.0115	0.0122	0.0117	0.0131
GBP	1.8141	1.4637	196.0400	1	2.2584	-	-	-
CHF	0.8030	0.6472	86.7600	0.4425	1	-	-	-
AUD	0.7553	0.6092	81.6100	-	-	1	0.9519	1.0669
CAD	0.7931	0.6397	85.6800	-	-	1.0494	1	-
NZD	0.7075	-	76.4400	-	-	0.9362	-	1

As an instructive example of the sensitivity analysis, suppose that the exchange rate r_{54} ($= 0.4425$) changes to $r_{54}' = 0.4423$. That is, $\beta = 0.9995$. Since x_{54} is basic, from Case 2 in the previous section, with the subtree T_5 containing only node 5, and the subtree T_4 containing all other nodes; we will have the new reduced costs $\bar{c}_{5j}' = \bar{c}_{5j}^* - \log 0.9995$ for $j = 1, 2, 3, 4$, $\bar{c}_{i5}' = \bar{c}_{i5}^* + \log 0.9995$ for $i = 1, 2, 3, 4$, and other reduced costs unchanged.

Using Matlab to model the sensitivity analysis procedure, the above reduced costs were updated, the optimality check was done, re-optimization was deemed necessary and performed by the program to give us a new arbitrage cycle USD \rightarrow GBP \rightarrow EUR \rightarrow CHF \rightarrow USD.

6. Conclusion

In this work, we have applied the network simplex method to a BIP model to detect currency arbitrages. Using Matlab, we customized a program modelled on this method that can search for arbitrages among many commonly used currencies. As a numerical example, we demonstrated the use of our algorithm involving real-time online exchange rates. It is hoped that this approach to currency arbitrage detection will lead to future practical implementation.

Acknowledgements The author would like to thank Prof Ye Heng Qing for his valuable comments.

References

- [1] Gilat, Amos. 1994. *MATLAB: An Introduction with Applications*. Wiley, 2nd Edition.
- [2] Goldberg, A.V., Plotkin, S.A., and Tardos, E. 1991. Combinatorial algorithms for the generalized circulation problem. *Mathematics of Operations Research*, 16(2), 351-381.
- [3] Hillier, F. S., and Lieberman, G. J. 2005. *Introduction to Operations Research*. McGraw Hill, New York.
- [4] Soon, W. M., and Ye, H. Q. 2007. Currency arbitrage detection using a binary integer programming model. *Working paper*.
- [5] Vanderbei, Robert J. 2001. *Linear Programming: Foundations and Extensions*. Kluwer Academic Publishers.
- [6] The MathWorks: <http://www.mathworks.com/access/helpdesk/help/techdoc/matlab.shtml>

Locii Associated with Tangents and Normals of Conic Sections

Tilak de Alwis

talwis@selu.edu

Department of Mathematics
 Southeastern Louisiana University
 Hammond, LA 70403
 USA

Abstract: In this paper, we will investigate several locus problems associated with tangent lines and normal lines of conic sections. The conic sections we consider include parabolas and ellipses, but hyperbolas will be left to the reader. For example, given an arbitrary point P on one of these conic sections, consider the tangent line and/or the normal line to the conic at that point. One can form several regions bounded by these tangent lines, normal lines, other auxiliary lines, and the conic section itself. We are primarily interested in investigating the locus of the center of gravity of these regions as the point P moves along the conic section. The computer algebra system *Mathematica* was used to help with our computations.

1. Introduction

In this section, we will recall some standard facts about the center of gravity of a plane region. As a first case, consider the triangle in the XY -plane with vertices at the points (x_1, y_1) , (x_2, y_2) and (x_3, y_3) . The center of gravity G of this triangular region, also called centroid, is given by the following well-known formula (see [3]):

$$G = \left(\frac{x_1 + x_2 + x_3}{3}, \frac{y_1 + y_2 + y_3}{3} \right) \quad (1.1)$$

As another case, consider the region \mathfrak{R} bounded by the graphs of $y = f(x)$, $y = g(x)$, $x = a$, and $x = b$. Here we are assuming that a and b are real numbers such that $a < b$, and f and g are continuous functions such that $f(x) \leq g(x)$ on the interval $[a, b]$. See the following figure:

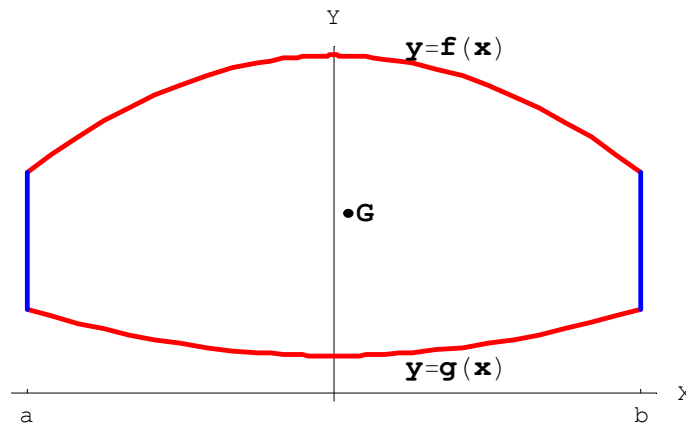


Figure 1.1 The Center of Gravity of a Region Bounded by Two Curves

The center of gravity $G(\bar{x}, \bar{y})$ of the region \mathcal{R} is given by the following equations (see [2]):

$$\bar{x} = \frac{\int_a^b x[f(x) - g(x)] dx}{\int_a^b [f(x) - g(x)] dx} \tag{1.2}$$

$$\bar{y} = \frac{\int_a^b \frac{1}{2}[f^2(x) - g^2(x)] dx}{\int_a^b [f(x) - g(x)] dx} \tag{1.3}$$

Similarly, if the region is bounded by the graphs of $x = f(y)$, $x = g(y)$, $y = c$, and $y = d$, where c and d are real numbers such that $c < d$, and f, g are continuous functions such that $g(y) \leq f(y)$ on the interval $[c, d]$, then the center of gravity of this region is given by integrals similar to (1.2) and (1.3). The main difference is that the integrals will be performed with respect to the y -variable, rather than x .

In the next section, we will consider the center of gravity of several types of regions associated with tangent lines and normal lines of a parabola.

2. Locus of the Center of Gravity of Regions Associated with Parabolas

(a) Consider the parabola given by $y^2 = 4ax$ where a is a nonzero constant. Any point on this parabola can be written as $P(at^2, 2at)$ where t is any real parameter. Let us first calculate the equations of the tangent line and the normal line to the graph at P : By differentiating both sides of the equation $y^2 = 4ax$ implicitly with respect to x , one can obtain $2y(dy/dx) = 4a$, which yields $dy/dx = 2a/y$ (see [2]). By evaluating this at $P(at^2, 2at)$, one can find the slope of the tangent line at P to be $1/t$. To find the equation of the tangent line, one can use the point-slope formula $y - y_1 = m(x - x_1)$. Thus, the equation of the tangent line at P is given by $y - 2at = (1/t)(x - at^2)$. By simplifying, the required equation of the tangent line is given by the following:

$$yt = x + at^2 \tag{2.1}$$

Now the slope of the normal line at P is given by $-t$, so its equation is given by $y - 2at = -t(x - at^2)$. Simplifying this leads to the following:

$$y = -xt + at^3 + 2at \tag{2.2}$$

Suppose the tangent line given by equation (2.1), and the normal line given by equation (2.2) intersect the X -axis at the points Q and R respectively, where $t \neq 0$. We are interested in finding

the locus of the center of gravity of the triangular region PQR , as the point P moves along the parabola. See the following figure:

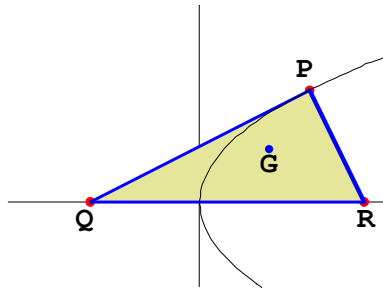


Figure 2.1 The Center of Gravity of the Region Bounded by the Tangent, Normal, and the x -axis

Using equations (2.1) and (2,2), it is easy to calculate the points Q and R to be $Q(-at^2, 0)$ and $R(at^2 + 2a, 0)$. Let $G(\alpha, \beta)$ be the center of gravity of the triangle PQR . Using the equation (1.1), one obtains the following equations:

$$\alpha = (at^2 + 2a) / 3 \tag{2.3}$$

$$\beta = 2at / 3 \tag{2.4}$$

In order to find the locus of G , we want to eliminate the t variable between the equations (2.3) and (2.4). The equation (2.4) implies that $t = 3\beta / (2a)$. Plug this back in equation (2.3) to get $3\alpha - 2a = a[(3\beta) / (2a)]^2$. Simplify this equation, and replace α and β respectively by x and y to obtain the following:

$$y^2 = \frac{4}{3} \left(x - \frac{2a}{3} \right) \tag{2.5}$$

The equation (2.5) above provides the equation of the locus of the center of gravity of the triangle PQR . Recall that any curve given by the general equation $(y - k)^2 = 4a(x - h)$ represents a horizontal parabola with vertex at (h, k) with focal length a (see [3]). Therefore, our locus is a parabola with vertex at $(2a/3, 0)$, with focal length $2a/3$.

The following diagrams indicate different positions of the triangles PQR and their centers of gravity G , along with the locus of the center of gravity:

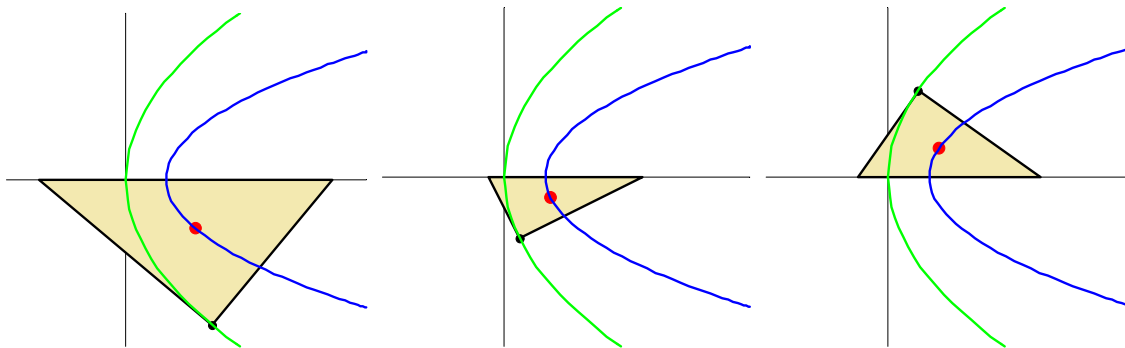


Figure 2.2 Various Positions of the Triangle PQR , its Center of Gravity G , and the Locus of G

(b) In this part, we will consider a second type of region associated with the tangent and the normal described in (a). Suppose that the tangent line and normal line at $P(at^2, 2at)$ meet the y -axis at S and T , respectively. We are now interested in investigating the locus of the center of gravity of the triangle PST for changing values of t . See the following figure:

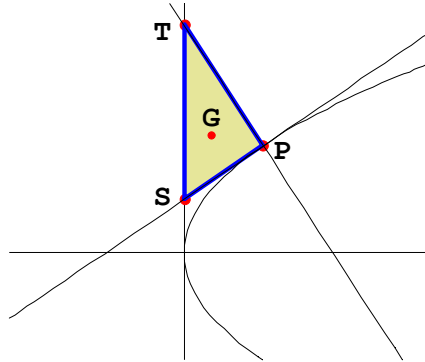


Figure 2.3 The Center of Gravity of the Region Bounded by the Tangent, Normal, and the y -axis

Let $G(\alpha, \beta)$ be the center of gravity of the triangle PST . Using the equations (2.1) and (2.2), it is easy to see that the coordinates of S and T are given by $(0, at)$ and $(0, at^3 + 2at)$ respectively. Again, using (1.1) one can obtain the coordinate of G as follows:

$$\alpha = at^2 / 3 \tag{2.6}$$

$$\beta = (at^3 + 5at) / 3 \tag{2.7}$$

By eliminating the t variable between the equations (2.6) and (2.7), we obtain the equation of the locus of G as follows:

$$y^2 = \frac{1}{3a} x(3x + 5a)^2 \tag{2.8}$$

Unlike the previous case (a), the locus given by equation (2.8) does not represent another parabola. To see the graph of (2.8), we will use the “**ImplicitPlot**” command of *Mathematica* (see [1] and [4]). What we have used was *Mathematica* 4.1 on a *Windows XP* platform. For the sample value of $a = 1$, the figure below shows the graph of the original parabola $y^2 = 4ax$ in black, and the graph of the locus given by equation (2.8) in red.

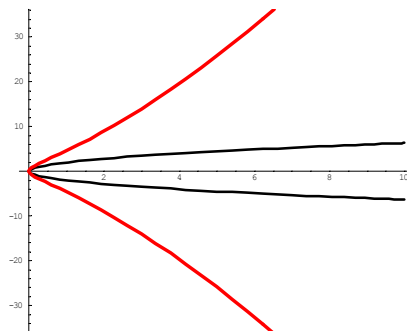


Figure 2.4 The Locus of the Center of Gravity of the Triangle PST (in red)

(c) We are now ready to consider a more interesting region arising from a parabola. Let \mathfrak{R} be the region bounded by the parabola $y^2 = 4ax$, the tangent line to the parabola at $P(at^2, 2at)$, and the x -axis. See the following figure:

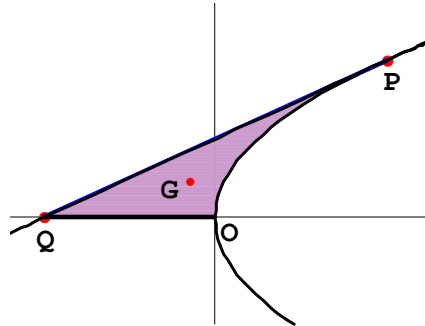


Figure 2.5 The C. G. of the Region \mathfrak{R} Bounded by the Parabola, Tangent, and the x -axis

We are interested in determining the locus of the center of gravity $G(\alpha, \beta)$ of the region \mathfrak{R} for changing values of t . However, unlike the previous regions discussed in (a) and (b), this region is not triangular, so one has to resort to integral calculus to calculate G . We will use equations very similar to (1.2) and (1.3), but it is more convenient to integrate with respect to the y -variable. Therefore, solve the equation of the parabola $y^2 = 4ax$ for x , and let $f(y) = y^2 / (4a)$. Likewise, solve the equation of the tangent line (2.1) for x , and let $g(y) = yt - at^2$. Then the coordinates of the center of gravity $G(\alpha, \beta)$ are given by the following equations:

$$\alpha = I_1 / I_3 \qquad \beta = I_2 / I_3 \qquad (2.9)$$

In the above, the integrals I_1, I_2 and I_3 are given by the following:

$$I_1 = \int_0^{2at} \frac{1}{2} [f^2(y) - g^2(y)] dy = \int_0^{2at} \frac{1}{2} \left[\frac{y^4}{16a^2} - (yt - at^2)^2 \right] dy \qquad (2.10)$$

$$I_2 = \int_0^{2at} y [f(y) - g(y)] dy = \int_0^{2at} y \left[\frac{y^2}{4a} - (yt - at^2) \right] dy \qquad (2.11)$$

$$I_3 = \int_0^{2at} [f(y) - g(y)] dy = \int_0^{2at} \left[\frac{y^2}{4a} - (yt - at^2) \right] dy \qquad (2.12)$$

It is tedious to calculate the integrals (2.10)-(2.12) by hand, so “**Integrate**” command of *Mathematica* comes to our rescue. Then, the “**Simplify**” command of *Mathematica* can be used to simplify the ratios given in equation (2.9), and the “**Eliminate**” command can be used to calculate the locus of the center of gravity $G(\alpha, \beta)$. The following simple *Mathematica* program achieves all these tasks (see [1], and [4]):

Program 2.1

```

Clear[a, t, y]
f[y_] := y^2 / (4 a);
g[y_] := y * t - a * t^2;
i1 = Integrate[(1 / 2) (f[y]^2 - g[y]^2), {y, 0, 2 a * t}];
i2 = Integrate[y (f[y] - g[y]), {y, 0, 2 a * t}];
i3 = Integrate[f[y] - g[y], {y, 0, 2 a * t}];
alpha = i1 / i3;
beta = i2 / i3;
Simplify[{alpha, beta}]
Eliminate[{x == alpha, y == beta}, t]
    
```

To execute the entire program, press “**Shift-Enter**” at the end of any command line. The program calculates the coordinates of the center of gravity G , and also the equation of the locus of G . The results are given below, respectively:

$$\alpha = -at^2/5 \quad \beta = at/2 \quad (2.13)$$

$$y^2 = -\frac{5a}{4}x \quad (2.14)$$

According to the equation (2.14), the locus of G is another parabola with vertex at $(0,0)$, and focal length $5a/16$. However, unlike the original parabola, the graph of the new parabola opens to the left.

One can also use *Mathematica* to create an animation of the center of gravity G . The following *Mathematica* program creates different positions of the region \mathfrak{R} , along with footprints of the center of gravity G :

Program 2.2

```

Clear[a, t, y, alpha, beta]
<< Graphics`ImplicitPlot`
a = 2;
f[y_] := y^2 / (4 a);
g[y_] := y * t - a * t^2;
i1 := Integrate[(1 / 2) (f[y]^2 - g[y]^2), {y, 0, 2 a * t}];
i2 := Integrate[y (f[y] - g[y]), {y, 0, 2 a * t}];
i3 := Integrate[f[y] - g[y], {y, 0, 2 a * t}];
alpha[t_] = Simplify[i1 / i3];
beta[t_] = Simplify[i2 / i3];
locus = Eliminate[{x == alpha[t], y == beta[t]}, t];
Do[ImplicitPlot[{y^2 == 4 a * x, locus}, {x, -8, 8},
  PlotRange -> {{-8, 8}, {-8, 8}}, PlotStyle -> {{Thickness[1 / 130]},
    {Thickness[1 / 180], RGBColor[0, 0, 1]}},
  Ticks -> None, Prolog -> {
    If[t < 0, {Thickness[1 / 100], RGBColor[0.972671, 0.949233, 0.707042]},
      Table[Line[{{f[y], y}, {g[y], y}}, {y, 2 a * t, 0, 0.1}],
      {Thickness[1 / 100], RGBColor[0.95314, 0.906264, 0.464851]},
      Table[Line[{{f[y], y}, {g[y], y}}, {y, 0, 2 a * t, 0.1}],
      {RGBColor[1, 0, 0], Thickness[1 / 100]},
        Line[{{a * t^2, 2 a * t}, {-a * t^2, 0}}]},
    {PointSize[1 / 40], RGBColor[0.6, 0.5, 0.9], Point[{a * t^2, 2 a * t}]},
    {PointSize[1 / 40], RGBColor[0.6, 0.5, 0.9], Point[{-a * t^2, 0}]},
    {PointSize[1 / 65], Table[Point[{alpha[s], beta[s]}], {s, -1.9, t, 0.2}]},
    {PointSize[1 / 50], RGBColor[1, 0, 0], Point[{alpha[t], beta[t]}]},
    {Thickness[1 / 100], Line[{{0, 0}, {-a * t^2, 0}}]} ]},
  {t, -1.9, 1.9, 0.2}]

```

A few frames of the animation are given below. Note that the locus of the center of gravity G of the region \mathcal{R} is given by the blue curve. The region \mathcal{R} is shaded in yellow, and the updated position of G can be seen as a red dot. The black dots are the previous positions of the center of gravity G .

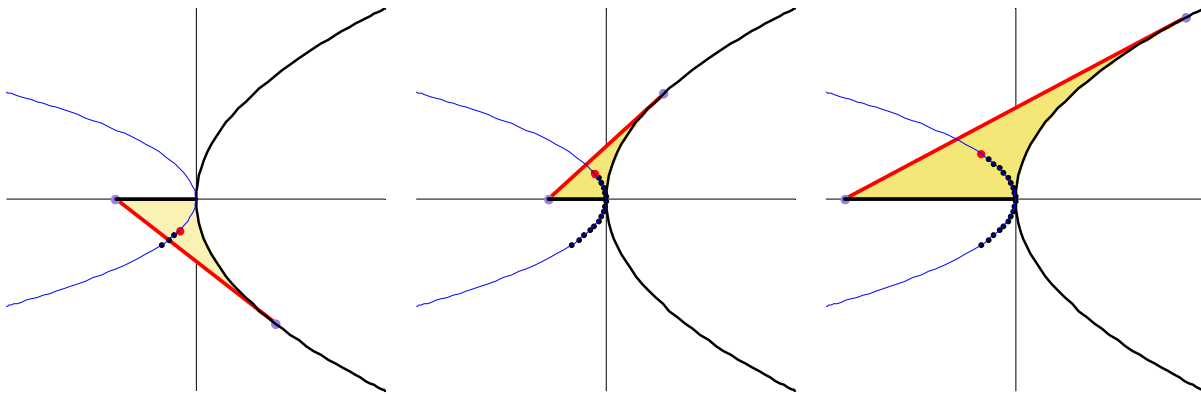


Figure 2.6 An Animation of the Center of Gravity of the Region \mathcal{R} , and its Locus (in blue)

3. Locus of the Center of Gravity of Regions Associated with Ellipses

In this section, we will investigate the locus of the center of gravity of regions associated with the tangents and/or normals of ellipses:

(a) Suppose a and b are positive real numbers such that $a \neq b$, and consider the ellipse given by the following equation:

$$\frac{x^2}{a^2} + \frac{y^2}{b^2} = 1 \quad (3.1)$$

Any point P on this ellipse (3.1) can be written as $P(a\cos\theta, b\sin\theta)$ where $0 \leq \theta < 2\pi$. By differentiating (3.1) implicitly with respect to x , one obtains that $2x/a^2 + 2y(dy/dx)/b^2 = 0$. Solving this equation for dy/dx , and evaluating at $P(a\cos\theta, b\sin\theta)$, one obtains the slope of the tangent line at P as $-(b\cos\theta)/(a\sin\theta)$. Then by using the point-slope formula, one can obtain the following equation of the tangent line to the ellipse (3.1) at point P :

$$\frac{x}{a}\cos\theta + \frac{y}{b}\sin\theta = 1 \quad (3.2)$$

Similarly, one can obtain the equation of the normal line to (3.1) at P as

$$\frac{x}{b}\sin\theta - \frac{y}{a}\cos\theta = \frac{\sin\theta\cos\theta}{ab}(a^2 - b^2) \quad (3.3)$$

In this part (a), we will investigate the locus of the center of gravity $G(\alpha, \beta)$ of the region bounded by the normal line at P , the x -axis, and the y -axis. See the following figure:

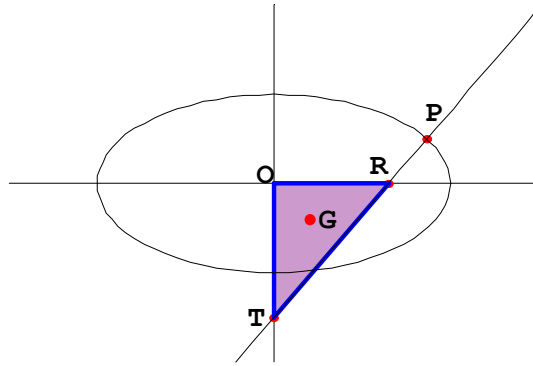


Figure 3.1 The Center of Gravity of the Region Bounded by the Normal and the Coordinate Axes

It is easy to calculate the coordinates of R and T as $R((a^2 - b^2)\cos\theta/a, 0)$ and $T(0, -(a^2 - b^2)\sin\theta/b)$. Then using equation (1.1), one can calculate the coordinates of the center of gravity G of the triangular region ORT to be the following:

$$\alpha = \frac{(a^2 - b^2)}{3a} \cos\theta \tag{3.4}$$

$$\beta = -\frac{(a^2 - b^2)}{3b} \sin\theta \tag{3.5}$$

Using the relationship $\sin^2\theta + \cos^2\theta = 1$, one can easily eliminate the variable θ between the equations (3.4) and (3.5). In this way, we obtain the equation of the locus of G as the following:

$$\frac{x^2}{A^2} + \frac{y^2}{B^2} = 1 \tag{3.6}$$

In the above $A = (a^2 - b^2)/(3a)$ and $B = (a^2 - b^2)/(3b)$. Since we assumed that $a > b$, it is clear that $A < B$. According to equation (3.6), the locus of G is an ellipse centered at the origin $(0, 0)$. Note that since $A < B$, the major axis of the ellipse will be along the y -axis. Let us also calculate the eccentricity of the new ellipse: Suppose e and E are the eccentricities of the original and the new ellipses. Then by definition of eccentricity, we have the following two equations (see [3]):

$$b^2 = a^2(1 - e^2) \tag{3.7}$$

$$A^2 = B^2(1 - E^2) \tag{3.8}$$

However, since $A = (a^2 - b^2)/(3a)$ and $B = (a^2 - b^2)/(3b)$, it can readily be seen that $A^2/B^2 = b^2/a^2$. Therefore, the equations (3.7) and (3.8) imply that $e = E$, which means that both ellipses have the same eccentricity.

We will below include both the graph of the original ellipse (3.1), and that of the locus of the center of gravity G , given by (3.6), for two sets of sample values, $a = 4, b = 2$ and also $a = 5, b = 2$:

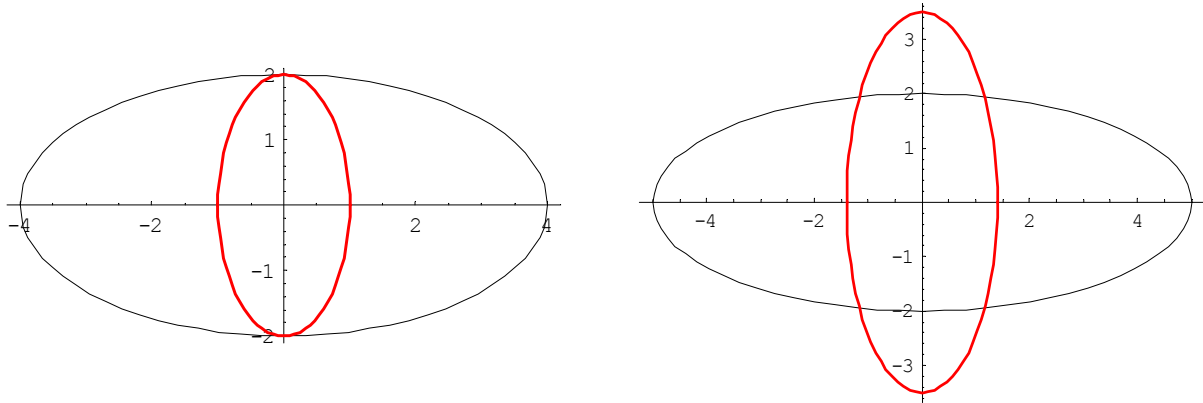


Figure 3.2 The Locus of the C.G. of the Triangle ORT – on left ($a = 4, b = 2$); on right ($a = 5, b = 2$)

The above discussion leads to the following theorem:

Theorem 3.1 Consider the ellipse given by $x^2/a^2 + y^2/b^2 = 1$ where a and b are distinct positive real numbers. Let P be any point on this ellipse, and let the normal line to the ellipse at P meet the x and y -axes at R and T respectively. Then the locus of the center of gravity of the triangular region ORT is another ellipse. The major axis of the new ellipse is perpendicular to the major axis of the original ellipse, and the two ellipses share the same eccentricity.

(b) Next we consider a non-triangular region associated with an ellipse: Let \mathfrak{R} be the region bounded by the ellipse (3.1), the tangent line at P , and the y -axis. We want to study the locus of the center of gravity $G(\alpha, \beta)$ of the region \mathfrak{R} , as the point P moves along the ellipse. See the following figure:

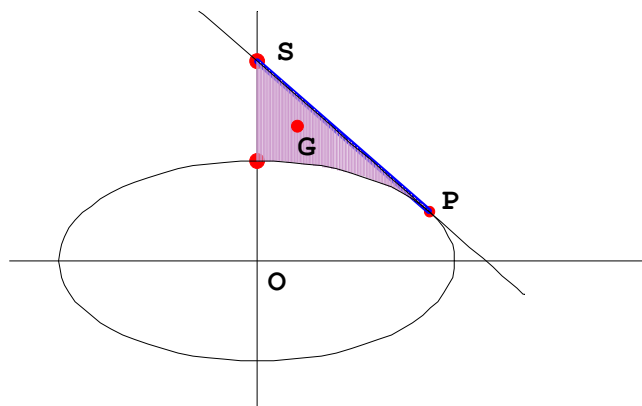


Figure 3.3 The C. G. of the Region \mathfrak{R} , Bounded by the Ellipse, Tangent, and the y -axis

In order to make the situation simpler, let us for the moment restrict P to be a point on the upper-half of the ellipse, i.e. we are assuming that $0 \leq \theta \leq \pi$. Solve the equation of the tangent line (3.2) for x , and let $f(x) = b \operatorname{Cosec} \theta (1 - x \operatorname{Cos} \theta / a)$. Similarly, solve the equation for the ellipse (3.1) for x , and let $g(x) = b \sqrt{a^2 - x^2} / a$. Here, we are only taking the positive square root, since $0 \leq \theta \leq \pi$. Then the coordinates of the center of gravity are given by the equations (1.2) and (1.3) where the limits of integration are from 0 to $a \operatorname{Cos} \theta$. The following *Mathematica* program, similar to Program 2.1, calculates G :

Program 3.1

```
Clear [a, b, theta]
f[x_] := b * Csc[theta] * (1 - x * Cos[theta] / a) ;
g[x_] := b * Sqrt[a^2 - x^2] / a ;
i1 = Integrate[ x (f[x] - g[x]) , { x, 0, a * Cos[theta] } ] ;
i2 = Integrate[ f[x]^2 - g[x]^2, { x, 0, a * Cos[theta] } ] / 2 ;
i3 = Integrate[ f[x] - g[x] , { x, 0, a * Cos[theta] } ] ;
alpha = i1 / i3 ;
beta = i2 / i3 ;
Simplify [{alpha, beta }]
```

Press “**Shift-Enter**” to execute the program, and *Mathematica* produces α and β . However, we further simplified these by hand, and obtained the following more simplified versions:

$$\alpha = \frac{-a(\operatorname{Sin} \theta - 1)^2}{[(\pi / 2 - \theta) \operatorname{Sin} \theta - \operatorname{Cos} \theta]} \tag{3.9}$$

$$\beta = \frac{b \operatorname{Cos}^3 \theta}{[-3(\pi / 2 - \theta) \operatorname{Sin}^2 \theta + 3 \operatorname{Sin} \theta \operatorname{Cos} \theta]} \tag{3.10}$$

Even with *Mathematica*, it is quite difficult to eliminate θ between the two equations (3.9) and (3.10). However, the above two equations provide the parametric equations of the locus of G . We can use the “**ParametricPlot**” command of *Mathematica* to graph the locus, along with the ellipse, as given below for $a = 2$ and $b = 1$ (see [4]):

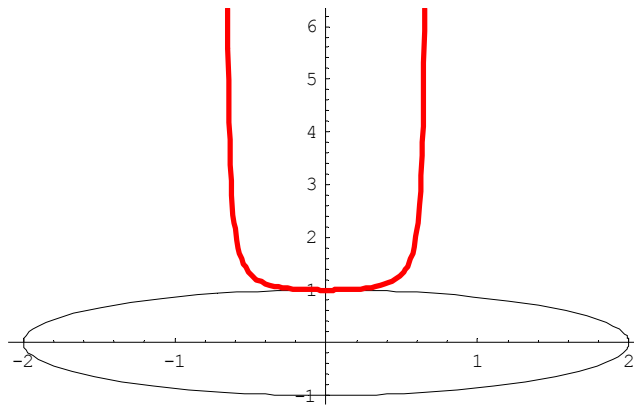


Figure 3.4 The Locus of the Center of Gravity of Region \mathfrak{R}

If the point P travels along the lower-half of the ellipse, the locus will be exactly the mirror image on the x -axis of the red curve given in the above figure. Anyhow, unlike in (a), this locus is not an ellipse.

4. Conclusion

In this paper, we considered several locus problems associated with tangents and normals of conic sections. Locus problems related to the center of gravity of a region are important not only to mathematics, but also to physics. As the region becomes more complicated, it is more convenient to use a computer algebra system to help with the computations. Computer algebra systems such as *Mathematica* can also be used to visualize the locus, via animations. Due to space limitations, we were unable to include several interesting regions arising from a hyperbola. The reader is encouraged to experiment with such regions, and discover new results. Armed with a suitable computer algebra system and a curious mind, the possibilities are almost endless!

References

- [1] Gray, T. and Glynn, J. (2000). *The Beginner's Guide to Mathematica, Version 4*. Cambridge, UK: Cambridge University Press.
- [2] Larson, H., Hostetler, R., and Edwards, B. (2002). *Calculus, 7th ed.* Boston, MA: Houghton Mifflin.
- [3] Loney, S. L. (1962). *The Elements of Coordinate Geometry*. London, UK: MacMillan.
- [4] Wolfram, S. (2003). *Mathematica Book, 5th ed.* Cambridge, UK: Cambridge University Press.